Tectonics

RESEARCH ARTICLE
10.1029/2021TC006707

**Key Points:**

- Late Eocene (37-34 Ma) crustal shortening in the Alboran Domain during formation of an Africa-verging orogenic wedge
- An Eocene age for the Alpine orogenic metamorphism must be considered for the geodynamic modeling of Western Mediterranean
- Brittle thinning of the Alboran Domain nappe stack is constrained at 18-17 Ma in the back-arc region of the Apennine-Maghrebian subduction

**Supporting Information:**

Supporting Information may be found in the online version of this article.

**Correspondence to:**

F. Rossetti,
federico.rossetti@uniroma3.it

**Citation:**

Marrone, S., Monié, P., Rossetti, F., Aldega, L., Bouybaouene, M., Charpentier, D., et al. (2021). Timing of Alpine orogeny and postorogenic extension in the Alboran Domain, inner Rif chain, Morocco. *Tectonics*, *40*, e2021TC006707. https://doi.org/10.1029/2021TC006707

Received 11 JAN 2021
Accepted 17 JUN 2021



# Timing of Alpine Orogeny and Postorogenic Extension in the Alboran Domain, Inner Rif Chain, Morocco

**Sara Marrone[1], Patrick Monié[2], Federico Rossetti[1], Luca Aldega[3], Mohamed Bouybaouene[4], Delphine Charpentier[5], Federico Lucci[1], David Phillips[6], Thomas Theye[7], and Mohamed Najib Zaghloul[8]**

[1]Dipartimento di Scienze, Università Roma Tre, Rome, Italy, [2]Géosciences Montpellier, Université de Montpellier, CNRS, Université des Antilles, Montpellier, France, [3]Dipartimento di Scienze della Terra, Sapienza Università di Roma, Rome, Italy, [4]Département de Géologie, Université de Rabat, Rabat, Morocco, [5]Chrono-Environnement, UMR 6249-CNRS, Université Bourgogne Franche-Comté, Besançon, France, [6]School of Earth Sciences, University of Melbourne, Parkville, VIC, Australia, [7]Institut für Anorganische Chemie, Universität Stuttgart, Stuttgart, Germany, [8]Département de Sciences de la Terre et d'Océanologie de l'Université "Abdel Maleek Essâdi" de Tanger, Tangier, Morocco

**Abstract** The variety of temporal and structural constraints on the Alpine tectonometamorphic signature of the metamorphic core of the Betic-Rif orogen (Alboran Domain) has supported a long-lasting debate regarding the Alpine tectonic and geodynamic evolution of the Western Mediterranean region. Uncertainty still exists on the timing and tectonic significance of (a) the Alpine orogenic construction; (b) exhumation of the deep roots of the orogen; and (c) transition from orogenic shortening to crustal extension. In this study, we address these major geological issues by focusing on the lower-grade units of the Alboran Domain (Upper Sebtides and Ghomarides) exposed in the Rif belt of northern Morocco. Through a multidisciplinary approach that integrates mesostructural and microstructural investigations with X-ray diffraction, quantitative mineral chemistry, and $^{40}Ar/^{39}Ar$ geochronology, a 20 Ma long tectonic history is reconstructed, which involves burial of the tectonic units at depth (late Eocene) and postorogenic exhumation under brittle conditions in the upper crust (early Miocene). We document a Priabonian (~37-34 Ma) $D_1/M_1$ progressive compressional deformation, during the formation of a SW-verging orogenic wedge (present coordinates), accreted toward the Africa plate. Brittle extensional detachment tectonics operated during the Burdigalian (~18-17 Ma), controlling the thinning of the previously structured Alboran Domain nappe stack and the final exhumation of the Alpine orogenic units. We propose that transition from orogenic build-up to collapse in the hinterland of the Betic-Rif orogen occurred when the retreat of the Apennine-Maghrebian subduction was efficient to drive transition from shortening to extension in the back-arc domain of the western termination of the Apennine-Maghrebian subduction zone.

## 1. Introduction

Orogeny is the process through which continental crust grows and differentiates at convergent plate margins. Understanding the tectonic structures and the temporal scales involved in the formation and the destruction of orogenic belts is the prerequisite to decrypt the geodynamic environments that control the transition from plate convergence to divergence and, ultimately, the cycles of continental assembly and breakup (e.g., Brown, 2010).

The study of the exhumed roots of the Alpine orogen in the Mediterranean region (Figure 1a) has fostered the advancement of knowledge on the geological processes and mechanisms operative during the transition from crustal shortening to extension at convergent plate margins (Dewey, 1988; Jolivet & Brun, 2010; Jolivet et al., 1998; Lister & Baldwin, 1993; Platt & Vissers, 1989). In particular, the dynamics of the Neotethyan subducting slab has been recognized to exert a primary role in controlling the stability of mountain belts, with crustal thinning largely controlled by back-arc extension caused by progressive slab retreat (e.g., Doglioni et al., 1997; Faccenna et al., 2004; Horvath et al., 1981; Jolivet & Brun, 2010; Jolivet & Faccenna, 2000; Jolivet et al., 1998, 2013; Malinverno & Ryan, 1986; Rosenbaum et al., 2002; Royden, 1993). Formation of Tertiary back-arc basins in the upper-plate of the retreating subduction imparted the first-order control on the physiography of the Mediterranean region. This resulted in a diffuse plate boundary where arcuate

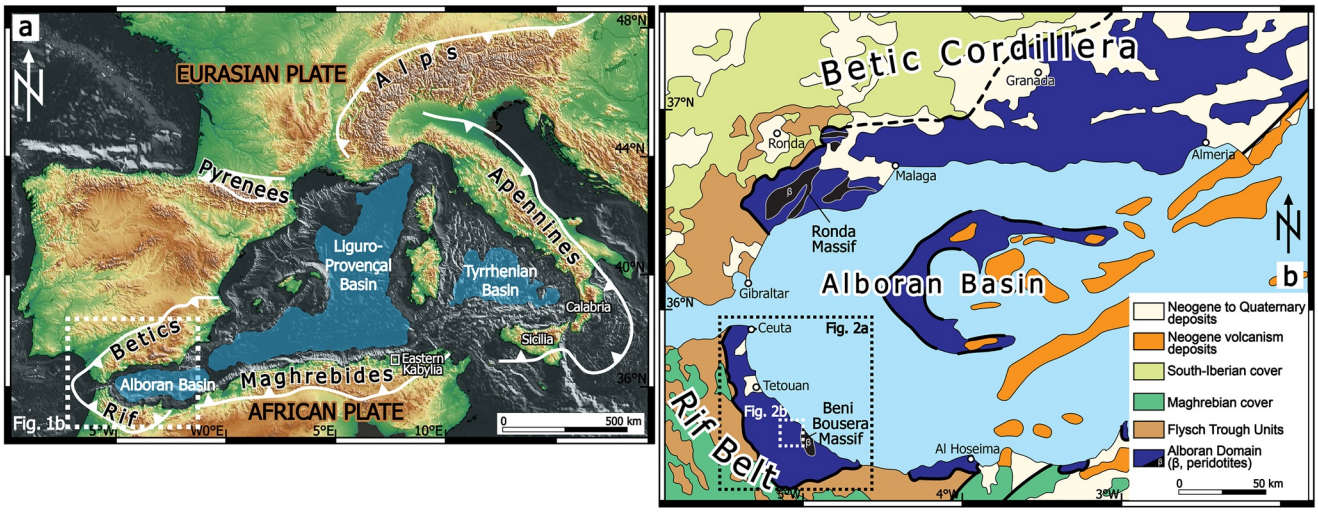


**Figure 1.** (a) The Western Mediterranean region showing the main Alpine orogenic belts and the distribution of the back-arc basins (modified after Faccenna et al., 2004). (b) Schematic geological map of the Betic-Rif orogen, showing distribution of the Alboran Domain in the hinterland domain (modified after Michard et al., 2006), with indication of the study area (dashed rectangle).

mountain belts are associated with localized and distributed continental rifts (Alboran, Liguro-Provençal, Tyrrhenian, Aegean basins), whose formation has coincided with active compression at the subduction fronts (Figure 1a).

The overprinting structures and the varying geothermal gradient (from low-temperature to high-temperature) associated with the back-arc (postorogenic) extension have usually obscured the early tectonometamorphic evolution associated with crustal thickening, hampering full assessment of the spatiotemporal scales and tectonic scenarios involved in orogenic construction. Consequently, there are large uncertainties in the tectonic reconstructions used to frame the geodynamic environment responsible for orogeny and crustal thickening in the region. This is clearly evident in the Western Mediterranean (Figure 1), where a widespread early Miocene thermal event is documented across the metamorphic hinterland of the Betic-Rif orogen (the so-called Alboran Domain; see Bessière et al., 2021 for a recent review) and debate continues in relation to the Alpine tectonometamorphic evolution of the Alboran Domain, with regard to: (a) the geodynamic scenario during consumption of the Neotethys ocean and formation of the Apennine-Maghrebian-Betic orogen, with models involving either double or single subduction scenarios (see e.g., Bessière et al., 2021; Carminati et al., 2012; Daudet et al., 2020; Faccenna et al., 2004; Handy et al., 2010; Lacombe & Jolivet, 2005; Leprêtre et al., 2018; Malusà et al., 2015; Molli & Malavieille, 2011; Pedrera et al., 2020; Platt et al., 2006; Romagny et al., 2020; Rosenbaum et al., 2002; van Hinsbergen et al., 2020; Vergés & Fernàndez, 2012; Williams & Platt, 2018); (b) the age of crustal thickening and thinning, including the role of structural inheritance (e.g., Acosta-Vigil et al., 2014; Augier et al., 2005; Gueydan et al., 2015; Homonnay et al., 2018; Li & Massonne, 2018; Massonne, 2014; Michard et al., 1997; Montel et al., 2000; Platt & Vissers, 1989; Platt & Whitehouse, 1999; Platt et al., 1998, 2005, 2006; Rossetti et al., 2010, 2020; Ruiz Cruz & Sanz De Galdeano, 2013; Sánchez-Navas et al., 2014, 2017; Sánchez-Rodríguez & Gebauer et al., 2000; Zeck & Whitehouse, 2002; Zeck & Williams, 2001); (c) the metamorphic conditions prevailing during late-orogenic extension (e.g., Azañón et al., 1998; Michard et al., 2006; Platt et al., 1998, 2003a, 2003b; Soto & Platt, 1999; Vidal et al., 1999); and (d) the tectonic evolution of the back-arc regions, with models showing continuous extension, pulses of shortening or transpressional shearing (e.g., Azañón & Crespo-Blanc, 2000; Balanyá et al., 1997; Booth-Rea et al., 2007; Frasca et al., 2017; Hidas et al., 2013; Garrido et al., 2011; Gueydan et al., 2019; Mazzoli & Martín-Algarra, 2011; Platt & Vissers, 1989; Platt et al., 2003a, 2003b; Rossetti et al., 2005).

The aim of this study is to provide time and structural constraints on the Alpine evolution of the Western Mediterranean region. Here, we focus on the lower-grade tectonic complexes of the Alboran Domain (Upper Sebtides and Ghomarides; Kornprobst, 1974; Michard et al., 2006) exposed in the Moroccan arm of

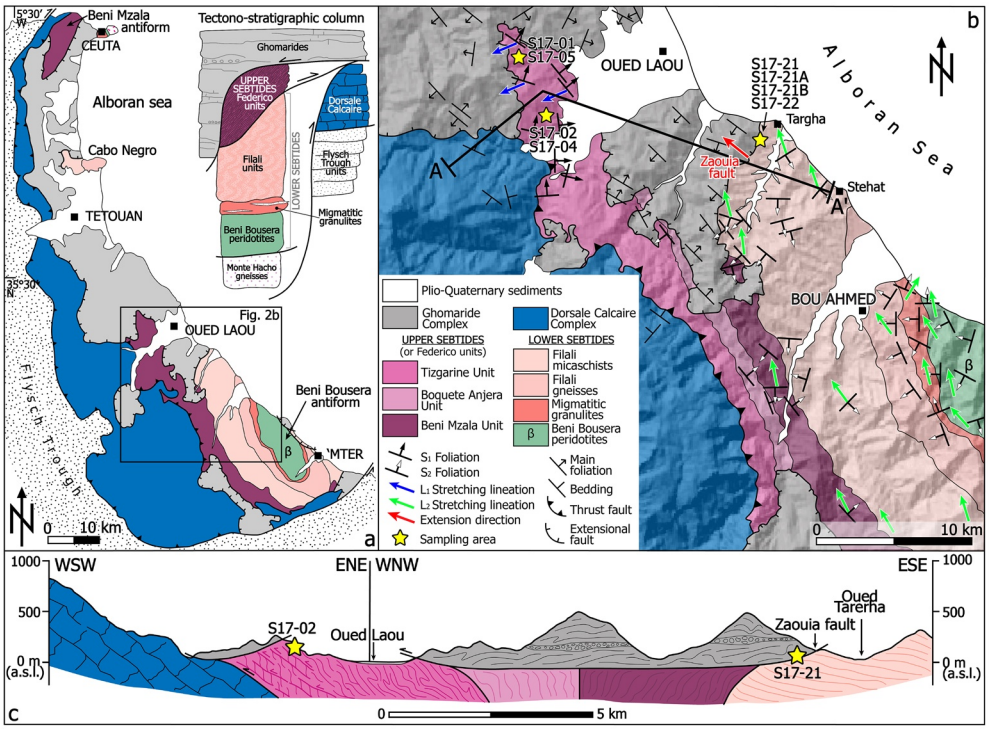


**Figure 2.** (a) Schematic geological map (modified and readapted after Kornprobst, 1974) of the Alboran Domain in the Rif belt, with location of the four tectonic windows where the Sebtide Complex crops out and with indication of the study area (black rectangle; modified after Kornprobst, 1974). The tectonostratigraphic column (not to scale; modified and readapted after Chalouan et al., 2008) shows the tectonic architecture of the Alboran Domain in the Rif (b) Structural map of the study area showing the distribution of the collected structural data and the sampling areas (structural data derived from Gueydan et al., 2015; Marrone et al., 2021; Michard et al., 2006 and this study). (c) Geological cross section illustrating the structural architecture of the study area, showing the abrupt truncation of the main Alpine regional foliation in the Sebtides units operated by the flat-lying Zaouia Fault, bounding the contact with the Ghomaride Complex at the fault hanging wall. The location of the samples used for Ar-Ar geochronology are also shown.

the Betic-Rif chain (Figure 2a). These tectonic complexes largely escaped the early Miocene postorogenic thermal relaxation that affected the Alboran Domain at regional scale and are assumed to better preserve vestiges of the orogenic processes, in the transition from crustal shortening to extension in the Western Mediterranean. A minimum time lapse of ca. 20 Ma is recognized between the syn-orogenic burial of the tectonic units at depth (late Eocene, at ca 37-34 Ma) and the postorogenic exhumation in the brittle crust (early Miocene, at ca. 18-17 Ma), providing ultimate constraints to the geodynamics of orogenic construction and destruction in the Mediterranean region.

## 2. Geological Background

The Betic-Rif arcuate belt of the western Mediterranean region is part of the peri-Mediterranean Alpine orogenic system, developed along the active margin formed during the Mesozoic-Cenozoic convergence between African and Eurasian plates (Figure 1a; e.g., Daudet et al., 2020; Dewey et al., 1989; Faccenna et al., 2004; Guerrera et al., 2019; Handy et al., 2010; Jolivet et al., 2003, 2008; Leprêtre et al., 2018; Lonergan & White, 1997; Platt, 2007; Platt et al., 2013; Romagny et al., 2020; Rosenbaum et al., 2002; van Hinsbergen et al., 2020). This orogenic domain experienced postorogenic collapse and crustal thinning during the early Miocene formation of the Alboran back-arc basin (e.g., Booth-Rea et al., 2007; Comas et al., 1999; Dewey, 1988; Faccenna et al., 2001, 2004; García-Dueñas et al., 1992; Jolivet & Faccenna, 2000; Monié et al., 1994; Platt & Vissers, 1989; Platt et al., 2003a, 2003b; van Hinsbergen et al., 2014; Vergés & Fernàndez, 2012; Zeck, 1996), in association with diffuse magmatism and high-temperature metamorphism (e.g., Esteban et al., 2011; Michard et al., 2006; Negro et al., 2006; Platt & Whitehouse, 1999; Platt et al., 2003a, 2003b;

Rossetti et al., 2010, 2013; Soto & Platt, 1999; Tubía et al., 1997, 2004; Turner et al., 1999). As a result, the orogenic roots were finally exhumed in the hinterland domains to form the metamorphic core (hinterland domain) of the Betic-Rif orogen, referred to as the Alboran Domain (Andrieux et al., 1971; Casciello et al., 2015; García-Dueñas et al., 1992; Michard et al., 2006; Platt et al., 2013) (Figure 1).

The Alboran Domain consists of continental-derived metamorphic units that can be correlated across the Betic-Rif chain (Figure 1; Balanyá & García-Dueñas, 1988; Chalouan & Michard, 2004; Chalouan et al., 2008; Didon et al., 1973; García-Dueñas et al., 1992; Kornprobst, 1974; Michard et al., 2006; Platt et al., 2013; Tubia et al., 1992). From bottom to top: (a) the high-pressure metapelites of the Nevado-Filabride Complex (e.g., Augier et al., 2005; Johnson et al., 1997; Li & Massonne, 2018; Monié et al., 1991; Platt et al., 2006; Puga et al., 1999), not exposed in Morocco, (b) the low-to high-grade Alpujarride-Sebtide Complex, enveloping the large peridotite bodies of Ronda and Beni Bousera (Azañón & Crespo-Blanc, 2000; Azañón et al., 1998; Balanyá et al., 1997; Bouybaouene et al., 1995; Gueydan et al., 2015; Kornprobst, 1974; Mazzoli & Martín-Algarra, 2011; Michard et al., 1997, 2006; Monié et al., 1991, 1994; Rossetti et al., 2010, 2020); and (c) the Malaguide-Ghomaride Complex, made up of low-grade Paleozoic basement rocks unconformably covered by discontinuous Mesozoic-Tertiary deposits (Chalouan & Michard, 2004; Kornprobst, 1974; Lonergan, 1993; Michard et al., 2006; Serrano et al., 2006). In both arms of the Betic-Rif orogen, the sedimentary Mesozoic-Cenozoic successions of the Dorsale Calcaire, the detached Mesozoic cover of the metamorphic units (Malaguides-Ghomarides and/or Alpujarrides-Sebtides), form the frontal tectonic zones of the hinterland domain and tectonically overlie the external fold-and-thrust belt (Chalouan & Michard, 2004; Kornprobst & Durand-Delga, 1985; Martín-Algarrra et al., 2004; Michard et al., 2006; Nold et al., 1981; Vitale et al., 2015; Wildi, 1983).

The Alpujarride-Sebtide Complex consists of a postmetamorphic nappe stack of tectonometamorphic units, characterized by a high-pressure/low-temperature (HP/LT), subduction-type metamorphism on Permian-Triassic protoliths and a high-grade, Barrovian-type metamorphism on pre-Alpine protoliths, respectively (Azañón et al., 1998; Bouybaouene et al., 1995; El Maz & Guiraud, 2001; Gueydan et al., 2015; Marrone et al., 2021; Michard et al., 2006; Rodríguez-Ruiz et al., 2019; Ruiz Cruz et al., 2010; Williams & Platt, 2018), typified by a marked increase in the peak temperature in the lower levels of the tectonic units (Álvarez-Valero et al., 2014; Argles et al., 1999; Azañón & Crespo-Blanc, 2000; Azañón et al., 1998; Balanyá et al., 1997; Barich et al., 2014; Booth-Rea et al., 2007; Comas et al., 1999; García-Casco & Torres-Roldán, 1999; García-Dueñas et al., 1992; Gueydan et al., 2015; Haissen et al., 2004; Michard et al., 2006; Monié et al., 1994; Negro et al., 2006; Platt et al., 2013; Rossetti et al., 2005, 2010, 2020; Sánchez-Navas et al., 2014, 2017; Soto & Platt, 1999; Tubía et al., 1997; Zeck et al., 1992). The thermal structure within the Alpujarride-Sebtides has been commonly attributed to the heat source provided by the intracrustal emplacement of the peridotite bodies (Ronda in the Betics and Beni Bousera in the Rif; Figure 1), which are tectonically interlayered within the continental metamorphic sequence of the Alpujarride-Sebtide Complex (e.g., Acosta-Vigil et al., 2014; Bessière et al., 2021; Frasca et al., 2017; Gueydan et al., 2019; Hidas et al., 2013; Mazzoli et al., 2013; Michard et al., 2006; Negro et al., 2006; Platt et al., 2013; Tubía et al., 1997). The rise of hot asthenosphere during extreme crustal thinning in the early Miocene has been also proposed to account for the low-pressure thermal metamorphism in the Alpujarride-Sebtides crustal units overlying the peridotites (Argles et al., 1999; Gueydan et al., 2015; Platt et al., 2003a).

### 2.1. Timing of the Alpine Orogeny in the Alboran Domain

Most of the Alpine geochronological and thermochronological data available for the Alboran Domain cluster, irrespective of the method, in the early Miocene (24-18 Ma time interval; see reviews in: Acosta-Vigil et al., 2014; Bessière et al., 2021; Gómez-Pugnaire et al., 2019; Homonnay et al., 2018; Michard et al., 2006; Platt et al., 2013; Rossetti et al., 2010, 2020; van Hinsbergen et al., 2020; Vergés & Fernàndez, 2012; Williams & Platt, 2018), obscuring the early orogenic tectonometamorphic fabrics. Consequently, the timing of the Alpine crustal thickening phase ($D_1$ deformation and $M_1$ metamorphism, $D_1/M_1$ event) and the associated HP/LT subduction-zone metamorphism in the Western Mediterranean is still largely debated. Relatively few and contradictory geochronological data are available for the Alpine $D_1/M_1$ stage in the region.

In the Betics, Eocene ages (ca. 50-40 Ma) have been proposed based on white mica $^{40}Ar/^{39}Ar$ geochronology on both the Alpujarrides (Bessière et al., 2021; Platt et al., 2005) and Nevado-Filabrides (Augier

et al., 2005), recently confirmed by electron microprobe dating of monazite from both the Alpujarride (Massonne, 2014) and Nevado-Filabride (Li & Massonne, 2018) complexes. Nonetheless, U-Pb zircon (López Sánchez-Vizcaíno et al., 2001), Lu-Hf garnet (Platt et al., 2006) and Rb/Sr multimineral isochron (Kirchner et al., 2016) geochronological data indicate a Miocene age (18-14 Ma) for continental subduction in the Nevado-Filabrides Complex. Accordingly, the Nevado-Filabride Complex is interpreted as the leading edge of the South-Iberian paleomargin, which underthrust the Alpujarride Complex at the early Miocene time (Behr & Platt, 2012; Booth-Rea et al., 2007; Daudet et al., 2020). In the Rif, $^{40}Ar/^{39}Ar$ white mica geochronology (Michard et al., 2006) from the Upper Sebtides and U-(Th)-Pb monazite dating (Homonnay et al., 2018) from the Lower Sebtides indicate a minimum age of ca. 28 Ma for the Alpine crustal thickening event in the region. Recently, Marrone et al. (2021) confirmed this scenario, providing evidence of ductile exhumation for the HP units, within the 29-21 Ma time period. A pre-Miocene timing for the Alpine orogenic tectonometamorphic evolution of the Alboran Domain is compatible with (a) the stratigraphic evidence of late Oligocene-early Miocene deposits (late Oligocene-Aquitanian Ciudad Granada Group and the Burdigalian Viñuela Group; Serrano et al., 2006), which, containing metamorphic clasts sourced from the hinterland, unconformably cover the Betic-Rif internal zone (Bourgois et al., 1972; Chalouan et al., 2008; Lonergan, 1993; Lonergan & Mange-Rajetzky, 1994; Martín-Algarrra et al., 2000; Serrano et al., 2006); and (b) the tectonostratigraphic and thermal evolution of the Cretaceous flysch basin of the Iberia paleomargin, where a Paleogene age for the onset of the Alpine crustal thickening has been recently proposed (Daudet et al., 2020).

To conclude, no firm time constraints exist in the Alboran Domain for (i) the Alpine crustal thickening event; and (ii) the transition from orogenic shortening to extension. The paucity of this primary information hampers refinement of the tectonic/geodynamic scenario during the Alpine orogeny in the Betic-Rif realm and, more generally, regional-scale correlations with other Mediterranean orogens.

### 2.2. The Alboran Domain in the Rif

The structural architecture of the Alboran Domain in the Rif belt is assigned to three main complexes of tectonic units, forming a postmetamorphic nappe stack thrust westward onto the external domains of the Rif chain; from top to bottom: Ghomaride, Sebtide and Dorsale Calcaire complexes (Chalouan & Michard, 1990; Chalouan et al., 2008; Kornprobst, 1974; Michard et al., 2006) (Figure 2a).

The Ghomaride Complex consists of pre-Alpine (Variscan) (Chalouan & Michard, 1990) metasedimentary basement units overlain by a discontinuous Mesozoic-Cenozoic sedimentary cover (Chalouan & Michard, 1990; Durand Delga & Kornprobst, 1963; Zaghloul et al., 2010). The tectonic juxtaposition of the Ghomaride units onto the Sebtides/Dorsale Calcaire nappe stack occurs along low-angle (detachment) extensional faults (Chalouan & Michard, 1990; Chalouan et al., 1997), which abruptly truncate the previously formed tectonic edifice. Among these faults, the Zaouia Fault is the best documented structure (Chalouan et al., 2008; Chalouan & Michard, 2004; Michard et al., 2006; Figure 2b). Results from Raman spectroscopy of carbonaceous material from the Paleozoic successions have documented a significant thermal resetting, with peak temperatures varying from ca. 500°C at the base down to <330°C at the top (Negro et al., 2006). This temperature gradient is consistent with the resetting of the K-Ar isotopic system during the Oligocene-Miocene, as documented in the lower part of the Akaili nappe of the Ghomarides, close to the Zaouia Fault (Chalouan & Michard, 1990, Figure 2b), where K-Ar white mica ages decrease downwards, from 183 Ma in the upper nappe to 25 Ma at its contact with the Filali micaschists of the Lower Sebtides (Chalouan & Michard, 1990). Ar-Ar biotite ages of ca. 21 Ma are also reported in the Filali micaschists immediately below the fault contact (Michard et al., 2006).

The Sebtide Complex crops out within four tectonic windows, at the core of roughly N-S trending antiformal structures, from north to south (Kornprobst, 1974; Michard et al., 2006): Beni Mzala, Ceuta, Cabo Negro, and Beni Bousera (Figure 2a). It is divided in the Upper Sebtides (Federico Units) and Lower Sebtides (Filali and Beni Bousera units), showing distinct tectonometamorphic signature and characterized by subduction-type and Barrovian-type metamorphic signature, respectively (Bouybaouene et al., 1995, 1998; El Maz & Guiraud, 2001; Goffé et al., 1996; Gueydan et al., 2015; Marrone et al., 2021; Michard et al., 1997, 2006; Negro et al., 2006; Rodríguez-Ruiz et al., 2019; Ruiz Cruz et al., 2010; Vidal et al., 1999).

The Lower Sebtides consist of felsic migmatitic granulites (kinzigites) forming the envelope of the Beni Bousera peridotites (together making up the Beni Bousera units; Álvarez-Valero et al., 2014; Bouybaouene et al., 1998; Haissen et al., 2004; Kornprobst, 1974; Melchiorre et al., 2017; Rossetti et al., 2010, 2020) passing upward to gneisses and micaschists of the Filali units (El Maz & Guiraud, 2001; Gueydan et al., 2015; Kornprobst, 1974). A polyphase tectonometamorphic evolution is documented in the Lower Sebtides, and still debated is the age of the climax of metamorphism, considered to be either Hercynian (Michard et al., 1997; Bouybaouene et al., 1998; Melchiorre et al., 2017; Montel et al., 2000; Rossetti et al., 2010, 2020) or Alpine (Early Miocene; Gueydan et al., 2015; Platt et al., 2003b) in age.

The Upper Sebtides (Federico units) are grouped into four low-grade tectonometamorphic units, composed of tectonic slices that experienced exclusively Alpine metamorphism and different peak P-T conditions ($D_1$/$M_1$ event) in the Alpine paleosubduction channel; from the uppermost to the lowermost: the Tizgarine (TZ), Boquete Anjera (BA), Beni Mzala-2 (BM2), and Beni Mzala-1 (BM1) units (Bouybaouene et al., 1995; Michard et al., 2006; Vidal et al., 1999). The Federico units are formed from the same lithostratigraphic sequence, which includes Permo-Triassic reddish to grayish phyllites, passing to Triassic quartzites and dolostones (Bouybaouene et al., 1995; Chalouan & Michard, 2004; Michard et al., 1997; Rodríguez-Ruiz et al., 2019; Vidal et al., 1999; Zaghloul, 1994). Peak $M_1$ metamorphism (Bouybaouene et al., 1995; Goffé et al., 1996; Michard et al., 2006; Vidal et al., 1999) varies from LP/LT (0.3–0.4 GPa and 300°C) for TZ ($M_1$ peak paragenesis: cookeite-pyrophyllite-phengite) to HP/LT, eclogite-facies (1.3–1.8 GPa, 450–550°C) conditions in BM units ($M_1$ peak paragenesis: Mg-carpholite-Mg-chloritoid, talc-phengite-kyanite). Each tectonic unit is thus characterized by its own peak P-T conditions, but overall exhibit nearly isothermal exhumation paths with final cooling within the low greenschist facies conditions (Bouybaouene et al., 1995; Marrone et al., 2021; Michard et al., 2006; Vidal et al., 1999).

The Dorsale Calcaire complex consists of tectonic slices made of Triassic-lower Jurassic shallow water carbonates, evolving upward into Cretaceous slope and basin deposits, with no evidence of Alpine metamorphic overprint (El Kadiri et al., 1992; Fallot, 1937; Maaté, 1996; Mattauer, 1960; Michard et al., 2006; Nold et al., 1981). A main Aquitanian-late Burdigalian shortening stage is documented, responsible for the WSW verging thrusting and tectonic imbrication onto the Flysch domain (Vitale et al., 2015; Zaghloul et al., 2005).

The available geochronological data for the Alpine HP/LT $D_1$/$M_1$ event in the Rif are primarily derived from the BM units of the Upper Sebtides, where K-Ar and $^{40}Ar/^{39}Ar$ clay-mica mixtures, muscovite and biotite geochronology (Michard et al., 2006) and in situ $^{40}Ar/^{39}Ar$ white mica geochronology (Marrone et al., 2021), provided minimum ages ranging from late Oligocene (ca. 29-25 Ma) to the early Miocene (ca. 24-20 Ma). Early Miocene ages were also obtained from U-(Th)-Pb dating of allanite-rich epidotes and phosphates (light REE accessory minerals) in the Federico units of the Upper Sebtides (Janots et al., 2006). Ductile structures in both Upper (Federico units) and the Lower (Filali micaschists) Sebtides exposed in the Beni Mzala antiform (Figure 2a) are characterized by a pervasive post-$D_1$/$M_1$, $S_2$-$L_2$ planolinear tectonic fabric, with a dominant top-to-the-NNW (present coordinates) sense of shear (Gueydan et al., 2015; Marrone et al., 2021; Michard et al., 2006; Negro et al., 2006), which has been referred to the late Oligocene syn-orogenic exhumation of the deep-seated Federico units (Marrone et al., 2021). Similarly, Homonnay et al. (2018), based on integrated U-(Th)-Pb monazite and $^{40}Ar/^{39}Ar$ muscovite geochronology in the Lower Sebtides exposed in the Ceuta area (Figure 2a) proposed a minimum age of ca. 28 Ma for the syn-metamorphic Alpine thrusting and an Early Miocene (ca. 21 Ma) age for the postorogenic crustal thinning.

The late-orogenic exhumation of the Alboran Domain is primarily constrained by low-temperature thermochronology as derived from the Lower Sebtides, where zircon and apatite fission track data provided early Miocene ages, ranging from ~20 to ~15 Ma (Azdimousa et al., 2014). The apatite (U-Th)/He thermochronology from the same group of units yielded similar Aquitanian-Burdigalian ages, documenting rapid cooling and exhumation in the upper crust for the Alboran Domain during the early middle Miocene (Münch et al., 2021; Romagny et al., 2014). New $^{40}Ar/^{39}Ar$ illite Burdigalian-Serravallian (ca. 19-12 Ma) ages from extensional fault gouges cutting across the Lower Sebtides units of the Ceuta area (Figure 2a) were reported recently, constraining the timing of the Neogene brittle extensional tectonics in the hinterland of the Betic-Rif orogen (Münch et al., 2021).

**Table 1**
*List of the Studied Samples, With Geographical Location and Analytical Method Adopted*

| | | | Location | | | Analytical method | | |
|---|---|---|---|---|---|---|---|---|
| Sample | Unit | Rock type | Latitude (°N) | Longitude (°W) | Mineralogy | EMPA | XRD | $^{40}Ar/^{39}Ar$ step-heating |
| S17-01 | Tizgarine Unit | Qz-Cb vein | 35°24′22″ | 5°9′30″ | Qz-Cb-Ms-Chl-Prl | X | | |
| S17-02 | Tizgarine Unit | Fine-grained metapelite | 35°23′36″ | 5°9′10″ | Wm-Prl-Chl-Qz-Hem | X | X | X |
| S17-04 | Tizgarine Unit | Coarse-grained metapelite | 35°23′36″ | 5°9′10″ | Wm-Prl-Chl-Qz-Hem | X | X | |
| S17-05 | Tizgarine Unit | Coarse-grained metapelite | 35°24′22″ | 5°9′30″ | Wm-Prl-Chl-Qz-Hem | X | X | |
| S17-21 | Zaouia Fault | Fault gouge | 35°23′50″ | 5°1′40″ | Qz-Ms-Chl-Ab-Kln-Gp-Cal + Py | | X | |
| S17-21A | Zaouia Fault | Fault gouge | 35°23′50″ | 5°1′40″ | Qz-Ms-Chl-Ab-Kln + Gp | | X | |
| S17-21B | Zaouia Fault | Fault gouge | 35°23′50″ | 5°1′40″ | Qz-Ms-Chl-Ab-Kln-Gp-Cal-Py | | X | X |
| S17-22 | Zaouia Fault | Fault gouge | 35°23′50″ | 5°1′40″ | Qz-Ms-Chl-Ab-Kln-Cal | | X | |

*Note*. (*)Mineral abbreviations after Whitney and Evans (2010); Wm: white mica.

## 3. Materials and Methods

Our study was conceived to constrain the timing and tectonic structures responsible for the Alpine orogenic and postorogenic evolution of the Alboran Domain in the Rif. To achieve this goal, we focused on the NW flank of the Beni Bousera antiform, where the TZ unit of the Upper Sebtides is thrust over the Dorsale Calcaire and is in tectonic contact with the overlying Ghomaride nappe stack along the Zaouia Fault, part of the extensional detachment systems bounding the base of the Ghomaride Complex (Figures 2a and 2b).

Although the Alpine metamorphism in TZ unit is of LP/LT type, as indicated by the assemblage Prl-Sud-Cook and the absence of (Fe-Mg)-carpholite ($P < 0.6$ GPa and $T \sim 300$°C; Bouybaouene et al., 1995; Goffé et al., 1996; Jolivet et al., 1998; Vidal & Goffé, 1991; Vidal et al., 1992, 1999), these rocks were deformed under high $P/T$ gradient conditions (~10°C/km). The TZ unit appears to have escaped the early Miocene tectonothermal event that overprinted and reset geochronometers in deeper units (see Homonnay et al., 2018; Marrone et al., 2021; Michard et al., 2006; Rossetti et al., 2010, 2020). This unit likely experienced temperatures lower than the closure temperature of white micas for argon diffusion (mainly in the range 350–450°C in most metamorphic contexts depending on grain size, cooling rate, and pressure; Harrison et al., 2009), therefore potentially preserving white mica crystallization ages. Therefore, the TZ unit is used as a proxy to refine the timing and deformation regimes of the Alpine orogeny, whilst the tectonic structure and age of the Zaouia extensional fault serves as a proxy to refine timing of the brittle Alpine postorogenic tectonics in the Alboran region.

Field work was carried out to define the structural architecture of the study area (Figure 2b). Selected rock samples, representative of the different textures recognized in the field (see Table 1 for the sample location and description), were chosen for petrographical investigation through optical, scanning electron microscopy (SEM), and electron microprobe analysis (EMPA). SEM and X-ray powder diffraction (XRD) analyses were combined to identify and quantify mineral phases in the samples and to determine the white mica polytypes (e.g., Dalla Torre et al., 1994). Step-heating $^{40}Ar/^{39}Ar$ geochronology on different mica grain-size fractions (<0.2, 0.2–0.5, 0.5–2, >2 μm) is used to constrain the timing of deformation in the studied samples.

Details on the analytical methods and protocols adopted in this study are provided in Text S1–S5 in supporting information. Mineral abbreviations are after Whitney and Evans (2010), complemented with Wm for white mica and Cook for cookeite (lithium-bearing chlorite).

## 4. Results

The TZ unit is widely exposed on the western limb of the Beni Bousera antiform (Figure 2a), where the Upper Sebtides define a verticalized zone of tectonic units located between the Dorsale Calcaire units to the west and the Filali micaschists of the Lower Sebtides to the east. This assembly of metamorphic rocks

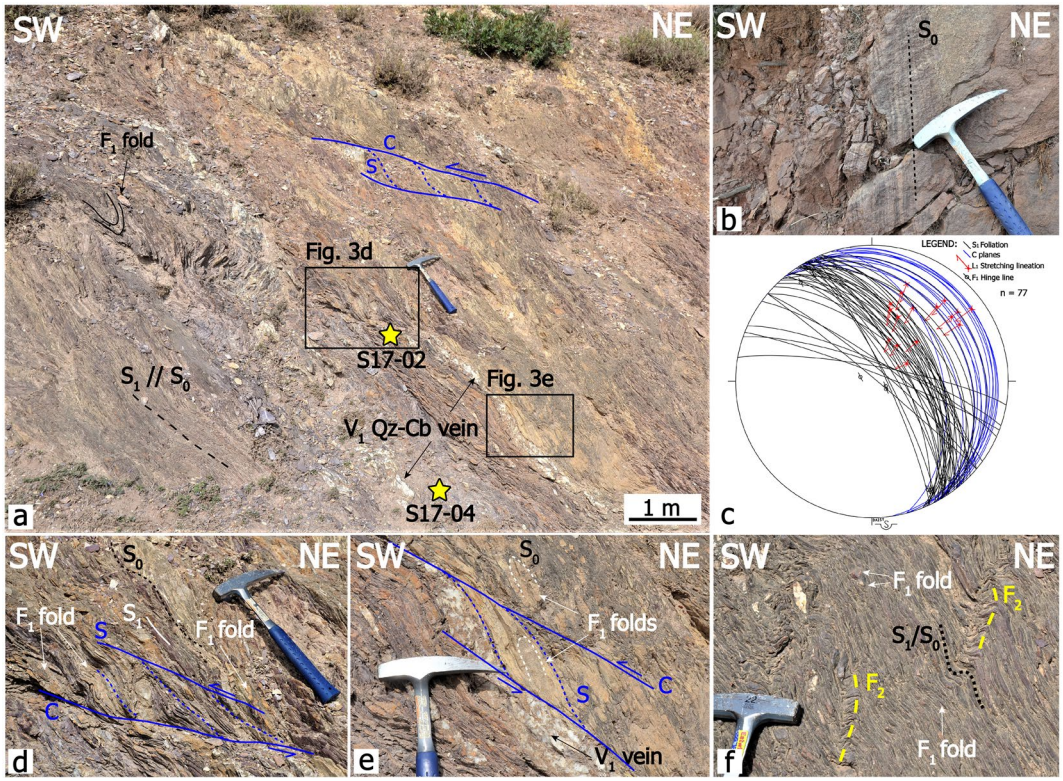


**Figure 3.** Outcrop-scale structural setting of the Tizgarine Unit. (a) $S_1$ foliation associated with isoclinal $F_1$ folds and Qz-Cb $V_1$ veins. Distributed S-C tectonites point to top-to-the-SW sense of shear (exposure parallel to $L_1$ and normal to $S_1$, X-Z section of the $D_1$ finite strain ellipsoid). (b) Primary ($S_0$) foliation preserved within the $D_1$ shear lithons. (c) Stereoplot (lower hemisphere equal-area projection) showing the attitude of the collected $D_1$ structural elements. The red arrows indicate the tectonic sense of transport (movement of the hanging wall block) as deduced in S-C tectonites. (d, e) Detail of the kinematic criteria showing top-to-the-SW shearing in S-C tectonites. $F_1$ folds and $V_1$ are sheared along top-to-the-SW shear bands. (f) Late, subvertical, NW-SE striking $F_2$ kink bands deforming the $S_1$ foliation.

is cut by a sub-horizontal brittle extensional fault (Zaouia Fault), bounding the contact with the overlying Ghomaride nappe stack (Figures 2b and 2c).

### 4.1. Tizgarine Unit: Deformation Fabrics and Studied Samples

The Tizgarine unit consists of alternating fine-grained and coarse-grained metapelite layers, interbedded with quartzites and conglomerates (see also Rodríguez-Ruiz et al., 2019). The unit is tectonically superimposed onto the Dorsale Calcaire units along an east-dipping tectonic contact (Figure 2c). At the meso-scale, the structural fabric of the Tizgarine unit consists of a pervasive, syn-metamorphic fabric ($D_1/M_1$), with $S_1$ and $S_1$-$L_1$ tectonites and associated $V_1$ syn-metamorphic Qz-Cb vein segregations. The veins are usually deformed, folded and transposed along the $S_1$ foliation (Figure 3a). Despite usually transposed by the $D_1$ deformation, the primary sedimentary layering ($S_0$) can be recognized in the field (Figures 3a and 3b).

The $S_1$ foliation consists of a disjunctive cleavage striking NW-SE, dipping at high-angle toward the NE (50–70°) and forming the axial surface of isoclinal $F_1$ folds with nearly horizontal hinge lines. The $L_1$ stretching lineations are WSW-ENE trending (Figure 3c) and composed of Qz-Wm ± Chl ± Cb associations. Distributed zones (up to 50 cm thick) of shear strain localization are often observed, with development of S-C tectonites defined by centimeter-to-decimeter spaced C shear planes. On exposures parallel to $L_1$ and orthogonal to $S_1$ (X-Z section of the finite strain ellipsoid), the S-C fabric and the $F_1$ fold vergence consistently point to a top-to-the-SSW sense of shear (Figures 3a, 3d, and 3e). The composite $D_1/M_1$ fabric is further deformed by meso-scale upright $F_2$ folds and kink bands, with axial surfaces ($S_2$) striking subparallel to the $S_1$ foliation (Figure 3f).

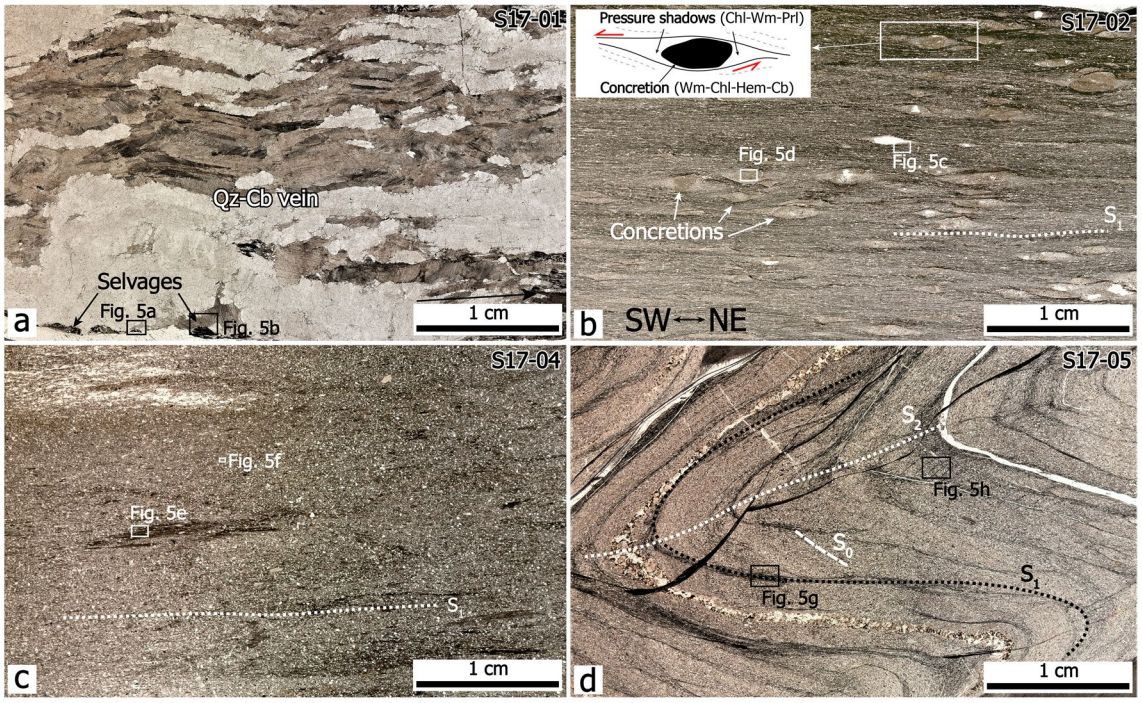


**Figure 4.** Thin section scan images of representative samples of the Tizgarine unit. (a) Qz-Cb $V_1$ (vein; sample S17-01), with indication of the metamorphic selvage shown in Figures 5a and 5b. (b) Oriented metapelite sample (S17-02), showing a continuous $S_1$ foliation wrapping around Cb-Wm-Chl-Hem concretions (see Figures 5c and 5d). The sense of shear as deduced by oblique foliation and asymmetric pressure shadows indicate top-to-the-SW sense of shear (exposure parallel to $L_1$ and normal to $S_1$). (c) Coarse-grained metapelite sample (S17-04) showing a disjunctive foliation ($S_1$), with indication of the areas investigated through back scattered electron (BSE) imaging. (d) Coarse-grained metapelite sample (S17-05) showing the hinge zone of a $F_2$ fold (see Figure 3 for location), and incipient development of a crenulation cleavage affecting the $S_0$ and $S_1$ foliations (see Figures 5g and 5h).

Four samples (S17-01, $V_1$ vein and selvage, S17-02, S17-04, and S17-05; Table 1 and Figures 3a and 4) were collected to investigate the detrital and syn-metamorphic mineralogy (through SEM, XRD, and EMPA) and microtexture. The $M_1$ syn-metamorphic assemblage as observed in the selvages surrounding the $V_1$ veins (Figure 4a) is composed of Wm-Prl-Chl-Qz-Hem (see also Bouybaouene et al., 1995; Goffé et al., 1996; Rodríguez-Ruiz et al., 2019). Significantly, Cook and Sud chlorites (see below) coexist with Wm and Prl in the paragenesis (Figures 5a and 5b).

Sample S17-02 is a metapelite (Figure 4b), collected within a $D_1$ top-to-the-WSW shear band. At the thin section scale, in section cuts orthogonal to $S_1$ and parallel to $L_1$, the sample shows a continuous $S_1$ foliation, wrapping around Cb-Wm-Chl-Hem concretions (Figures 5c and 5d). Asymmetric pressure shadows surrounding the concretions indicate top-to-the-SW sense of shear (Figure 4b). Samples S17-04 and S17-05 are coarse-grained metapelites (Figures 4c and 4d). At the thin section scale, the typical microfabric consists of a disjunctive slaty cleavage (Figures 5e, 5g, and 5h), where the phyllosilicate-rich (M-domains) and quartz-feldspar (QF-domains) layering can be recognized. The M-domains are defined by layers (up to 2–10 μm thick) of Fe-oxides (Hem) and newly formed (syn-tectonic) metamorphic Wm (here after referred to as $Wm_m$) + Prl ± Chl, wrapping around (up to 500 μm in size) microlithons dominantly composed of lozenge-shaped QF-domains (Figure 5g), with subordinate carbonate and Wm (detrital Wm, referred to as $Wm_d$) ± Rt, Ap, Zrn, Tur. Quartz grains are typically flattened by intracrystalline deformation, with tails typically formed by $Wm_m$ + Chl aggregates. Notably, large $Wm_d$ grains are strained along the $S_1$ foliation, with fine-grained $Wm_m$ crystallizing in the low strain zones (Figures 5e and 5f). A spaced crenulation cleavage is usually observed at the $F_2$ hinge zones, folding the composite $S_0/S_1$ foliation (Figures 4d and 5h). The Qz microfabric, as reconstructed from the deformed $V_1$ vein (sample S17-01; Figure 4a), is dominated by ductile deformation textures, as indicated by sweeping undulose extinction, and with the recovery process indicated by deformation lamellae and subgrain formation. Evidence of dynamic recrystallization is documented by incipient bulging in the higher strained areas (Figure 6).

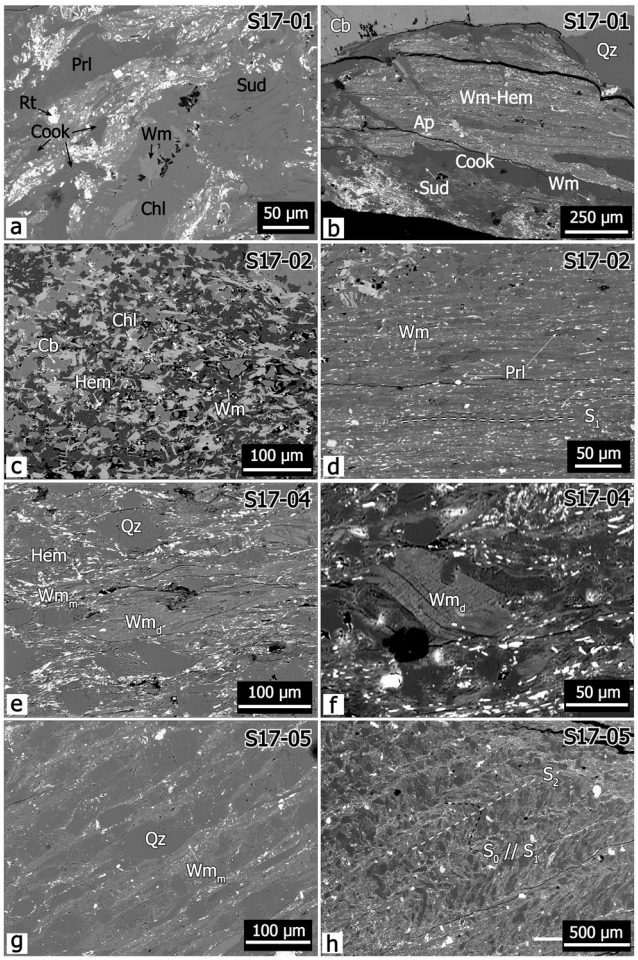


**Figure 5.** Microtextures of Tizgarine unit as revealed by BSE imaging. (a, b) Metamorphic selvages around the $V_1$ veins showing the $M_1$ metamorphic assemblage (Sample S17-01). (c) Detail of the Cb-Wm-Chl-Hem concretion in sample S17-02. (d) $S_1$ foliation defined by syn-kinematic Wm and Prl (Sample S17-02). (e) Detrital primary structure made of quartz (Qz) and white mica ($Wm_d$) grains enveloped by fine-grained syn-tectonic fine-grained white mica ($Wm_m$)-hematite (Hem) aggregates (Sample S17-04). (f) Detrital white mica fish preserved within the $S_1$ foliation (Sample S17-04). (g) Disjunctive, slaty $S_1$ foliation, with $Wm_m$-rich domains wrapping around flatted Qz (Sample S17-05). (f) Superimposed foliation caused by $D_2$ crenulation cleavage affecting the composite $S_0/S_1$ fabric (Sample S17-05). Mineral abbreviations after Whitney and Evans (2010).

Sample S17-02 was selected to constrain the age of the $D_1/M_1$ Alpine event through $^{40}Ar/^{39}Ar$ white mica geochronology, due to the penetrative character of the $D_1/M_1$ fabric and a minimal $Wm_d$ component.

### 4.2. The Zaouia Fault: Structural Architecture and Studied Samples

At Cape Zaouia (Figure 2a), a shallowly (30°) NW-dipping, up to 3-m-thick fault core separates the Ghomaride units at the fault hanging wall from the Filali micaschists of the Lower Sebtides at the footwall, with the complete tectonic elision of the Upper Sebtides (Figure 7a). The fault core consists of a gouge made of unconsolidated phyllosilicate-rich fine-grained material, pervasively cut by synthetic shear surfaces (Figures 7b and 7c). Fault kinematics documents a nearly pure dip-slip (extensional) motion (pitch angle of slickenlines: 90–100°; Figure 7d), indicating a general top-to-the-NW sense of shear, as deduced from drag pattern of foliations and synthetic Riedel shears within the fault gouge (Figure 7e). At the fault hanging wall, NE-SW synthetic and antithetic extensional fault systems are observed, accommodating a general NW-SE directed maximum extension direction. The fault rocks are dominated by foliated cataclasites, locally associated with dm-thick discontinuous fault gouges, wrapping around fault-bounded shear lenses (Figure 7f).

Four samples from the fault core (fault gouge) of the Zaouia Fault were collected for XRD analysis (S17-21, S17-21A, S17-21B, and S17-22; Table 1) to define the gouge mineralogy, and one representative sample (S17-21B) was used to constrain the age of faulting through $^{40}Ar/^{39}Ar$ geochronology.

### 4.3. XRD Analysis

The whole-rock XRD results for both the Tizgarine (S17-02, S17-04, and S17-05) and Zaouia Fault gouge (S17-21, S17-21A, S17-21B, and S17-22) samples are shown in Table 2.

The Tizgarine metapelite samples are mainly composed of Qz (33–65 wt.%) and Wm (Ms; 13–17 wt.%), with variable Prl (7–32 wt.%) and subordinate amounts of Hem (5–10 wt.%) and Chl (1–9 wt.%), Rt (up to 2 wt.%) and Kln (up to 1 wt.%). Carbonate minerals such as Dol (4 wt.%) and Cal (3 wt.%) have been observed in sample S17-05.

The Zaouia Fault gouge shows a mineralogical assemblage made up of Qz (10–22 wt.%), Wm (Ms; 37–45 wt.%), Chl (20–22 wt.%), and Ab (7–21 wt.%) as main mineral phases, with minor amounts of Kln (<4 wt.%) and Cal (<1 wt.%). Occasionally, gypsum is observed in sample S17-21B (18 wt.%), whereas Cal reaches amounts up to 7 wt.% in sample S17-22.

### 4.4. White Mica Polytypes

In order to characterize Wm polytypes, randomly oriented specimens for the fractions 50-2, 2–0.5, 0.5–0.2 µm of sample S17-02 (Tizgarine unit), and 2–0.5, 0.5–0.2, and <0.2 µm of sample S17-21B (Zaouia Fault gouge) were prepared. Results are shown in Table 3 and Figure 8. The reflection peaks at 3.88, 3.73, 3.49, 3.20, 2.99, 2.86, and 2.79 Å correspond to the $2M_1$ Wm polytype. The occurrence of 1M Wm polytype was confirmed by the reflection peaks at 4.12, 3.68, and 3.07 Å (Figure 8). The proportion of $2M_1$ and 1*M* polytypes was calculated by using the Rietveld refinement method and is presented in Table 3.

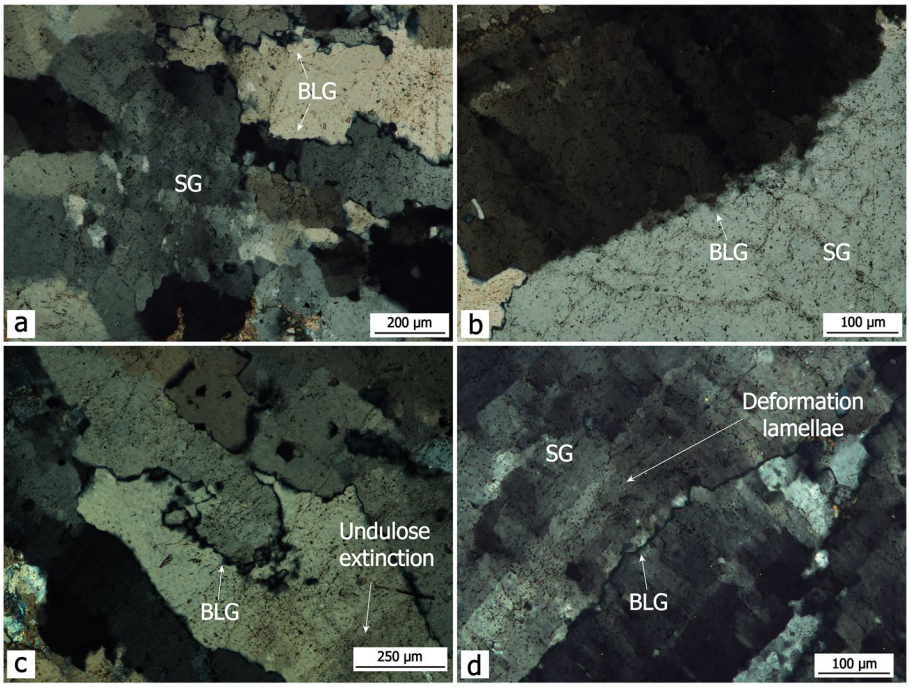


**Figure 6.** (a–d) Qz microfabric of sample S17-01 (Qz-Cb vein), showing evidence of ductile creep as indicated by sweeping undulose extinction, deformation lamellae and subgrain (SG) formation (crossed polars). Dynamic recrystallization textures are indicated by incipient bulging recrystallization (BLG).

The results indicate that both polytypes are present in all the fractions of the Tizgarine unit sample (S17-02). The $2M_1$/1M ratio increases with decreasing grain size, from 40% to 65%. In the Zaouia Fault gouge sample (S17-21B), the $2M_1$ is the almost unique Wm polytype (more than 90 wt.%) in the coarsest fraction. However, the $2M_1$ and 1M polytypes are present in broadly the same proportion in the <0.5 µm fractions.

### 4.5. Mineral Chemistry

Mineral compositions of the metapelite samples from the Tizgarine unit and calculated mineral formulae are presented in Table S1.

Detrital muscovite $Wm_d$ ($n = 17$) is characterized by $SiO_2$ ranging 45.90–48.22 wt.%, corresponding to 3.05–3.17 Si atoms per formula unit (apfu). The related ($Fe^{2+}$+Mg) ranges from 0.03 to 0.23 apfu. Calculated portions of end-members are $X_{Ms} = 0.56–0.80$, $X_{Cel} = 0.06–0.19$, $X_{Prl} = 0.00–0.16$, $X_{Pg} = 0.05–0.17$ (Figure 9).

The syn-metamorphic $Wm_m$ population ($n = 32$) shows $SiO_2$ ranging 46.27–49.22 wt.%, resulting in 3.11–3.24 Si apfu. ($Fe^{2+}$+Mg) is 0.04–0.21 apfu. End-members: $X_{Ms} = 0.44–0.71$, $X_{Cel} = 0.12–0.27$, $X_{Prl} = 0.03–0.27$, $X_{Pg} = 0.03–0.15$ (Figure 9). The considerable scatter can be attributed to mixtures of detrital and metamorphic white micas. However, it is evident from Figure 9 that $Wm_d$ and $Wm_m$ form two distinct groups, with the detrital group (Si = 3.10 apfu in average) being clearly less silicic than the metamorphically formed phengite (Si = 3.17 apfu in average).

Detected chlorite group minerals consist of (i) trioctahedral chlorite (Chl), (ii) sudoite (Sud), and (iii) cookeite (Cook). Chl ($n = 16$) is intermediate chamosite-clinochlore with a broad range of composition. Si ranges between 2.53 and 2.80 apfu, and $X_{Mg}$ from 0.22 to 0.58 (with $X_{Mg} = [Mg/(Mg + Fe^{2+})]$ atomic ratio). The thermometry model of Cathelineau and Nieva (1985), based on the $Al^{[IV]}$ content, indicates temperatures in the range 272–329 ± 15°C (average 306°C, $n = 16$). Sud ($n = 8$) contains slightly more than 3.0 Si apfu, and is relatively rich in Fe, with calculated $X_{Mg}$ of 0.83–0.86. The Cook composition ($n = 5$) is comparable to that reported from the Alpujarride-Sebtide Complex investigated by Goffé et al. (1996). Noteworthy

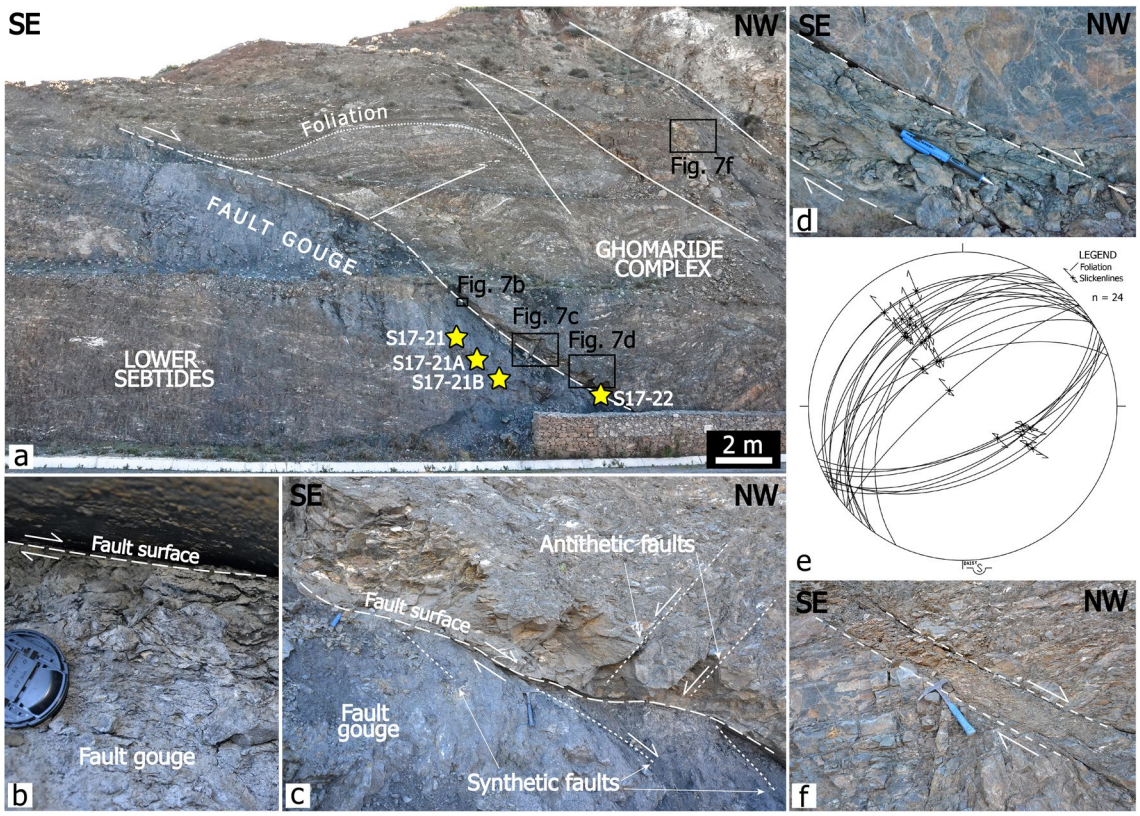


**Figure 7.** Outcrop-scale structural setting of the Zaouia Fault. (a) The Zaouia Fault as exposed along the road cut of the National Road 16. The road cut is trending nearly orthogonal to the slickenlines found on the fault surfaces. A discontinuous, up to 3-m-thick fault gouge is observed. The fault controls the contact between the Filali micaschists (Lower Sebtides) at the footwall and the Ghomaride Complex at the hanging wall, respectively. A set of synthetic, NW-dipping extensional fault systems are observed at the fault hanging wall. (b) Detail of the fault gouge. (c) SE-dipping antithetic fault splays at the fault hanging wall dying out along the fault gouge. (d) Foliated fault gouge at the base of the fault hanging wall. C′-type shear bands document top-to-the-NW shearing. (e) Stereoplot (lower hemisphere equal-area projection) showing the attitude of the collected structural elements. The fault kinematic is nearly pure extensional dip-slip. (f) Synthetic fault strands at the fault hanging wall. Up to dm-thick fault gouge decorated the slip zone.

is the relatively high content of $FeO_{tot}$ 0.63–0.86 wt.% and MgO 0.45–0.95 wt.%, indicating minor solubility toward the Sud end-member.

Prl composition is always close to the end-member. Minor amounts of Na and K can be related to the presence of finely white mica intergrowth not resolvable with the EMPA (e.g., Martínez et al., 2010).

**Table 2**
*XRD Whole-Rock Composition of the Tizgarine Unit and the Zaouia Fault Gouge*

| | Mineral mode (wt.%) | | | | | | | | | | | |
|---|---|---|---|---|---|---|---|---|---|---|---|---|
| Sample | Qz | Ms | Prl | Hem | Chl | Kln | Dol | Cal | Rt | Ab | Py | Gp |
| S17-02 | 33 | 17 | 32 | 10 | 5 | 1 | – | – | 2 | – | – | – |
| S17-04 | 64 | 17 | 7 | 10 | 1 | – | – | – | 1 | – | – | – |
| S17-05 | 65 | 13 | – | 5 | 9 | – | 4 | 3 | 1 | – | – | – |
| S17-21 | 22 | 37 | – | – | 22 | 3 | – | 1 | – | 14 | Tr | 1 |
| S17-21A | 10 | 45 | – | – | 22 | 2 | – | - | – | 21 | – | Tr |
| S17-21B | 13 | 37 | – | – | 20 | 3 | – | 1 | – | 7 | 1 | 18 |
| S17-22 | 14 | 42 | – | – | 21 | 4 | – | 7 | – | 12 | – | – |

*Note.* (*)Mineral abbreviations after Whitney and Evans (2010).

**Table 3**
*Whole-Rock Composition of Various Grain-Size Fractions of Samples S17-02 (Tizgarine Unit) and S17-21B (Zaouia Fault)*

| Sample | Fraction (μm) | Mineral proportion (wt.%) | | | | Wm (wt.%) | 1M (wt.%) | $2M_1$ (wt.%) |
|---|---|---|---|---|---|---|---|---|
| | | 1M | $2M_1$ | Chl | Other minerals | | | |
| S17-02 | 2–50 | 39 | 25 | 10 | 26 | 64 | 61 | 39 |
| | 0.5–2 | 52 | 43 | 1 | 5 | 95 | 55 | 45 |
| | 0.2–0.5 | 34 | 61 | 2 | 2 | 96 | 36 | 64 |
| S17-21B | 0.5–2 | 3 | 48 | 16 | 36 | 51 | 6 | 94 |
| | 0.2–0.5 | 31 | 38 | 15 | 18 | 69 | 45 | 55 |
| | <0.2 | 17 | 20 | 27 | 38 | 37 | 46 | 54 |

### 4.6. $^{40}Ar/^{39}Ar$ Step-Heating Geochronology

For the TZ, step-heating experiments were carried out on a bulk Wm separate and on the four fractions (<0.2, 0.2–0.5, 0.5–2, and >2–50 μm) of sample S17-02 (see Figures 3 and 4b for the outcrop conditions and microtextural characteristics; Tables 2–3 for the mineralogical assemblage). The same grain-size fractions were used to date movement along the Zaouia Fault using the fault gouge sample S17-21B (see Figure 7 for the outcrop conditions; Tables 2–3 for the constituent mineralogy). The age spectra of the bulk and fractions of TZ are reported in Figure 10 and the age spectra of the fractions of the Zaouia Fault are shown in Figures 11a, respectively. The Ar-Ar data derived from the Wm fractions have been all corrected for $^{39}Ar$ recoil loss as obtained through vacuum encapsulation experiments (see Text S4) and a summary of the retention (RAs), total gas (TGAs) and maximum ages is presented in Table 4. The complete data set is presented in Tables S2 and S3.

#### 4.6.1. Tizgarine Unit (Sample S17-02)

The bulk Wm separates show discordant age spectra with an overall staircase shape and older ages for the bulk-grained and coarse-grained fractions compared to the finest fraction (<0.2 μm). Apparent ages for the bulk sample (Figure 10a) increase from a minimum value of 55.9 ± 0.2 Ma (1σ error) for 30% of the released $^{39}Ar$ to a maximum value of 265.2 ± 1.9 Ma obtained at the end of degassing. A TGAs of 117.9 ± 3.0 Ma has been calculated with all steps (Tables S2 and 4).

Age spectra of the four grain-size fractions are shown in Figure 10b. For each spectrum, the first step with a zero age represents the amount of $^{39}Ar$ lost by recoil during neutron irradiation and measured before the step-heating degassing of the sample. As usually observed in fine-grained samples (e.g., Abd Elmola et al., 2018; Clauer, 2013; Dong et al., 1995; Fitz-Díaz et al., 2016; van der Pluijm et al., 2001), the percentage of recoiled $^{39}Ar$ increases with decreasing grain size, from about 4.1% for the fraction 2–50 μm to 21.8% for the fraction <0.2 μm (Table 4). The shape of the age spectra is quite different, with the larger grain sizes showing the greatest age discrepancy between the beginning and end of degassing. Thus, the coarsest fraction (2–50 μm) shows apparent ages that increase steadily from about 30 Ma to 107 Ma, never reaching a plateau. In contrast, the finest fraction produces a relatively flat age pattern for about 45% of final degassing of the sample, with ages in the range 41–47 Ma. For the four fractions, TGAs are between 64.3 ± 0.1 Ma (2σ error) and 29.8 ± 0.2 Ma, with RAs between 67.0 ± 0.1 Ma and 38.0 ± 0.3 Ma. This last value is provided by the two finest fractions that contain the highest proportion of the $2M_1$ mica polytype. All the analyzed fractions and the bulk sample show small and variable amounts of $^{37}Ar$, probably due to contamination by calcite undetected by XRD analysis (Table 2). The amount of $^{38}Ar$ formed by neutron reaction on chlorine is also variable (Table S2) but tends to increase in the $2M_1$ rich finest fractions (<0.5 μm), suggesting more interaction of the tiny micas with fluids at the time of their (re)crystallisation compared to the coarser micas that remained unaffected by $^{38}Ar_{(Cl)}$ contamination.

#### 4.6.2. The Zaouia Fault Gouge (Sample S17-21B)

The four fractions display age spectra that strongly vary with grain size and do not resemble those derived from the Tizgarine sample, except for the finest fraction that provides relatively consistent ages at the end

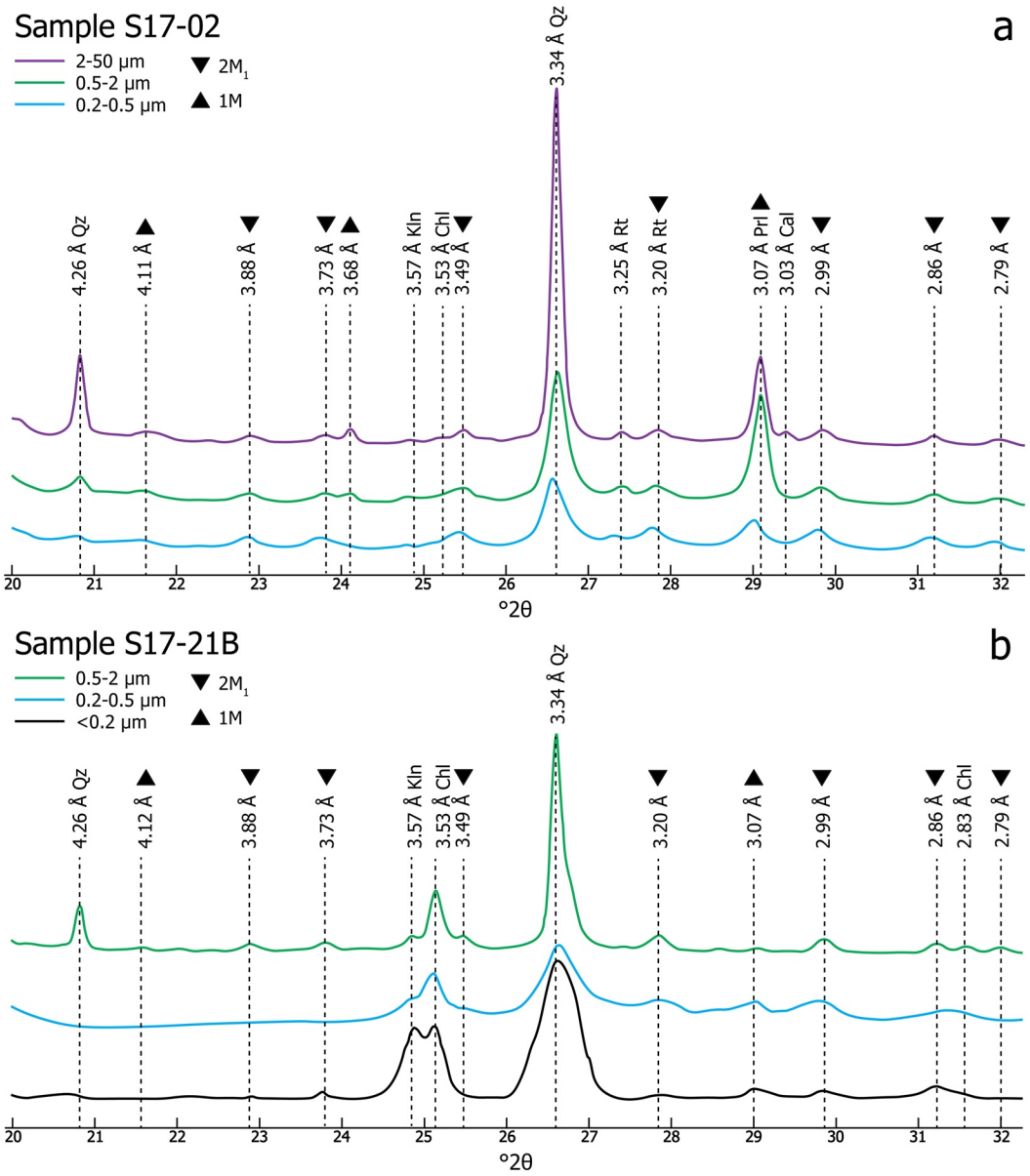


**Figure 8.** X-ray diffraction patterns for randomly oriented mounts for the different grain-size fractions and Wm polytype characterization. (a) Sample S17-02. (b) Sample S17-21B.

of argon degassing. The three other fractions (>0.2 µm) have hump-shaped age spectra, with maximum ages that increase toward the finest fraction (Figures 11a). Significantly, the coarsest fraction produced a very discordant age spectrum, with two successive "bumps" that may reflect complex recoil artifacts in a sample consisting mainly of quartz, chlorite, mica, and minor amount of kaolinite and gypsum (Table 2). It is worth noting, however, that the XRD data show an increase of the 1M mica polytype relative to $2M_1$ toward the finest fractions (Table 4). The amount of $^{39}Ar$ recoil loss is important and increases from 12.0% to 32.6% with decreasing grain size. TGAs show moderate dispersion and decrease with grain size from 21.0 ± 0.1 Ma to 18.4 ± 0.1 Ma (Figure 11a and Table 4). The RAs are inversely correlated with the grain size decrease and range from 27.3 ± 0.2 to 23.8 ± 0.1 Ma. The amount of $^{37}Ar$ formed by neutron reaction on calcium is variable but tends to be higher in the coarse fractions, probably due to the presence of gypsum in the sample (Table 2). The different fractions show a low content of $^{38}Ar_{(Cl)}$ that is mainly released during the first step-heating increments (Table S3).

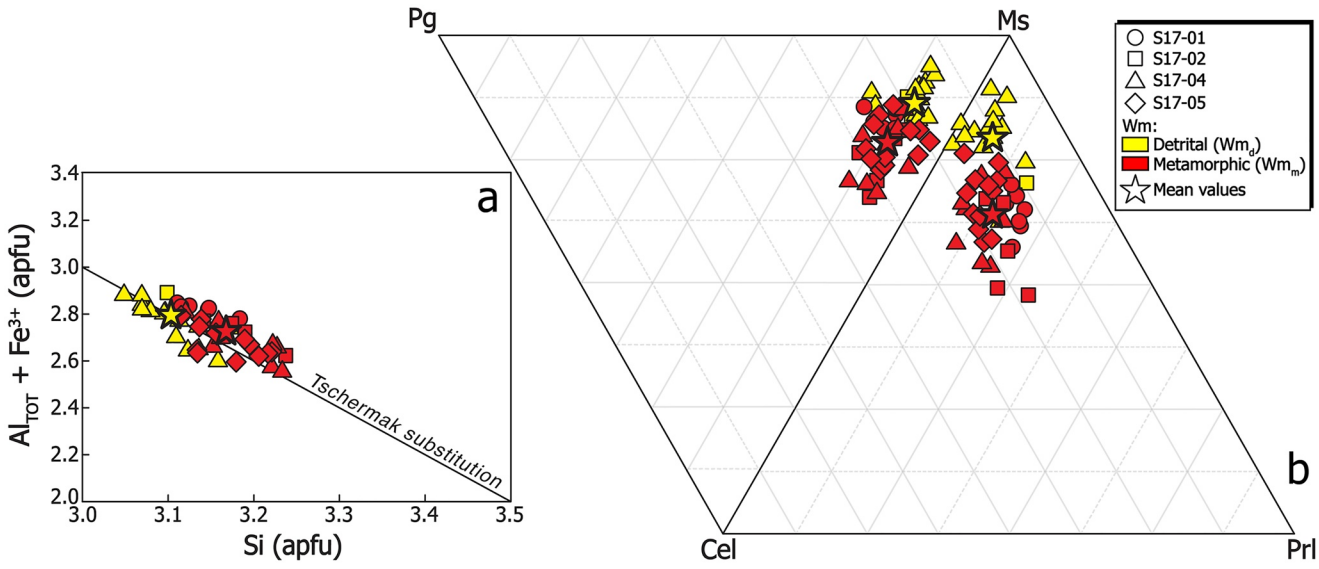


**Figure 9.** White mica compositions. (a) Si versus $Al_{TOT}$ + $Fe^{3+}$ diagram and (b) Ternary compositional diagrams, discriminating the analyzed $Wm_d$ and $Wm_m$ populations.

## 5. Discussion

The intense tectonometamorphic event associated with the ductile-to-brittle exhumation stage across the whole Alboran Domain of the Betic-Rif orogen resulted in the widespread transposition and overprinting of the early Alpine $D_1/M_1$ fabric (see e.g., Williams & Platt, 2018). Indeed, the existing literature describes the preservation of the Alpine $S_1$ foliation only in boudins or lens-shaped microlithons preserved within the penetrative (main) $S_2$ retrogressive (exhumation-related) foliation of the Alpujarride-Sebtide complex (Azañón et al., 1998; Azañón & Crespo-Blanc, 2000; Balanyá et al., 1997; Marrone et al.,2021; Michard et al., 2006; Platt et al., 2005; Rossetti et al., 2005; Simancas & Campos, 1993; Tubía et al., 1997; Williams & Platt, 2018).

The structural and petrographical investigations presented in this study indicate that the TZ unit of the Upper Sebtides in the Alboran Domain of the Rif belt experienced a first phase ($D_1$) Alpine deformation, syn-kinematic relative to low-grade $M_1$ metamorphism. The metamorphic peak was equilibrated at LP/LT metamorphic conditions ($P < 0.6$ GPa and $T \sim 300$°C; Bouybaouene et al., 1995; Goffé et al., 1996; Jolivet et al., 1998; Vidal & Goffé, 1991; Vidal et al., 1992, 1999), as further constrained by the Chl-thermometry. The Qz microfabric, documenting evidence of intracrystalline deformation and bulging recrystallization textures indicative of low-grade metamorphic conditions (below 400°C; Law, 2014; Passchier & Trouw, 2010; Stipp et al., 2002), is compatible with the thermal environment as derived from the $M_1$ metamorphic mineral paragenesis.

The $D_1$ fabric developed in response to a general SW-NE directed shortening regime, which evolved from ductile-to-brittle deformation during progressive top-to-the-SW shearing (present coordinates; Figures 2b and 3), compatible with overthrusting of the Federico units (Upper Sebtides) onto the Dorsale Calcaire (Figures 2b and 2c). Southwestward verging thrusting thus documents an Africa-directed tectonic vergence during orogenic shortening and nappe stacking in the hinterland domain of the Betic-Rif orogen. Dating the development of the syn-shearing $D_1/M_1$ tectonometamorphic fabric in the TZ unit (sample S17-02) thus provides the first opportunity to directly constrain the timing of the Alpine crustal thickening event in the Alboran Domain.

Moreover, the structural and temporal constraints derived from the study of the Zaouia Fault, one of the major extensional detachment fault zones that controls the brittle assembly of the Ghomaride Complex onto the Alpine metamorphic nappe stack (Chalouan et al., 2008; Chalouan & Michard, 2004; Michard

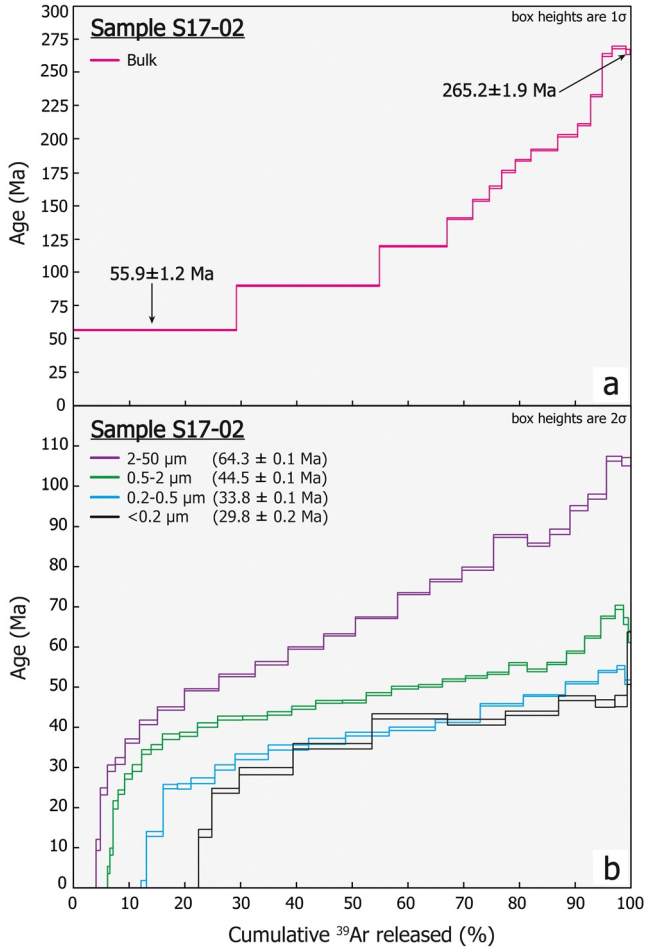


**Figure 10.** $^{40}Ar/^{39}Ar$ step-heating results for sample S17-02. (a) Age spectra for the bulk Wm. (b) Age spectra for the different grain-size fractions.

et al., 2006, Figure 2) can be used to refine the timing of activation of the postorogenic extensional detachment tectonics in the Alboran Domain of the Rif chain.

### 5.1. Age of the Alpine $D_1/M_1$ Orogenic Event

The discordant age spectrum provided by the bulk Wm separates from sample S17-02 (Figure 10a) suggests that at least two different age components contribute to the argon release, respectively, of Variscan and Alpine age. These two ages end-members are constrained by the maximum and minimum ages recorded by the age spectrum at 265 Ma and 56 Ma, respectively (Figure 10a). This evidence indicates that the dated metapelite sample, for which potassic Wm is the only source of radiogenic argon, contains different argon reservoirs with a large age range, which renders their interpretation challenging. Another complication comes from the fact that the micas formed at the time of $D_1/M_1$ shearing have a small grain size, which requires the use of adapted separation techniques, mineral characterization and vacuum encapsulation of the samples to monitor the amount of $^{39}Ar$ recoil loss in the different fractions.

The preservation of a detrital Variscan muscovite ($Wm_d$) in the Permo-Triassic metapelites of the Upper Sebtides is consistent with the polyphase evolution of the Alboran Domain and evidence of the orogenic Variscan belt on the margins of the western Mediterranean (e.g., Acosta-Vigil et al., 2014; Álvarez-Valero et al., 2014; Bouybaouene et al., 1998; Gueydan et al., 2015; Michard et al., 1997; Montel et al., 2000; Rossetti et al., 2013, 2020; Ruiz Cruz & Sanz de Galdeano, 2014; Sánchez-Navas et al., 2014, 2017; Zeck & Williams, 2001). In the Mediterranean region, similar exposures of Permo-Triassic continental-derived siliciclastic deposits that make up the TZ unit and, more in general the Alpujarride-Sebtide Complex, are widespread in Europe and Mediterranean region, formed from dismantling of the Variscan orogen during the onset of the Tethyan ocean rifting (Aldinucci et al., 2008; Díez et al., 2005; Linol et al., 2009; López-Gómez & Arche, 1993). In the Betics and Pyrenees,

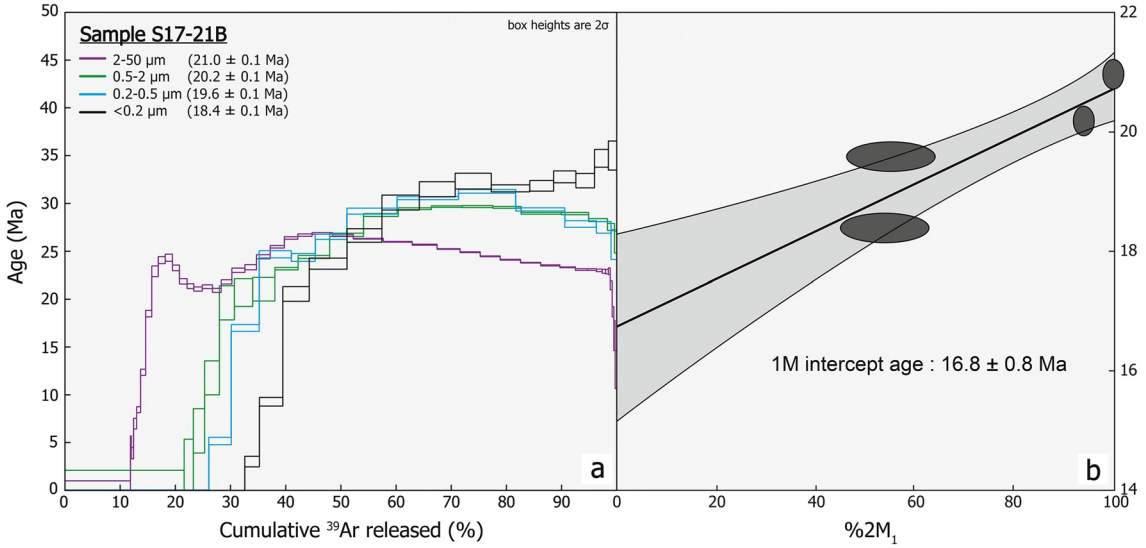


**Figure 11.** (a) $^{40}Ar/^{39}Ar$ step-heating results for sample S17-21B, showing the age spectra for the different grain-size fractions. (b) $\%2M_1$ versus age plot.

**Table 4**
*Summary of the $^{40}Ar/^{39}Ar$ Data and Wm Polytype Proportions for Samples S17-02 and S17-21B*

| Sample | Grain size (μm) | % Wm | $2M_1/1M$ | RA (Ma) | TGA (Ma) | Maximum age (Ma) | $^{39}$Ar recoil (%) | ICT (nm) | XCA (Ma) |
|---|---|---|---|---|---|---|---|---|---|
| S17-02 (Tizgarine Unit) | Bulk | 17 | – | – | 117.9 ± 1.5 | 268.5 ± 2.0 | – | | – |
| | 50–2 | 19 | 39/61 | 67.1 ± 0.1 | 64.3 ± 0.1 | 106.8 ± 0.6 | 4.07 | | – |
| | 2–0.5 | 37 | 45/55 | 47.4 ± 0.1 | 44.5 ± 0.1 | 69.9 ± 0.5 | 6.14 | | – |
| | 0.5–0.2 | 50 | 64/36 | 38.4 ± 0.1 | 33.8 ± 0.1 | 54.6 ± 0.5 | 12.14 | 22–26 | 36.8 ± 0.2 |
| | <0.2 | >60 | 67/33 | 38.0 ± 0.3 | 29.8 ± 0.2 | 47.3 ± 0.6 | 21.78 | 8–15 | 34.4 ± 1.1 |
| S17-21B (Zaouia Fault) | 50–2 | – | – | 23.8 ± 0.1 | 21.0 ± 0.1 | 26.9 ± 0.1 | 11.95 | | – |
| | 2–0.5 | 29 | 94/6 | 25.4 ± 0.2 | 20.2 ± 0.3 | 29.7 ± 0.1 | 21.69 | 40–50 | 25.2 ± 0.1 |
| | 0.5–0.2 | 24 | 55/45 | 26.5 ± 0.1 | 19.6 ± 0.1 | 31.2 ± 0.2 | 26.14 | 30–40 | 25.7 ± 0.1 |
| | <0.2 | 25 | 54/46 | 27.3 ± 0.2 | 18.4 ± 0.1 | 35.0 ± 1.5 | 32.59 | 10–25 | 25.6 ± 0.3 |

$^{40}Ar/^{39}Ar$ dating of coarse micas in these metapelites provided age spectra similar to that obtained on the bulk metapelite of Tizgarine (Abd Elmola et al., 2018), thus confirming the large-scale depositional environment of these Permo-Triassic rocks.

The minimum age of 56 Ma given by the first heating step of the bulk Wm concentrate is interpreted as a maximum age limit for the age of the Alpine $D_1/M_1$ event. The analysis of the age spectra of the four Wm fractions <50 μm, when combined with the XRD results, provides better constraints on this event. With decreasing grain size, these fractions show a constant proportion of pyrophyllite (30–36%), a decreasing amount of quartz (32-3%), an increasing content of white mica (19–60%) and an enrichment of $2M_1$ polytype relative to 1M polytype (Tables 2–4). The presence of the latter is probably related to the diagenetic evolution of the Permo-Triassic pelites before their Alpine metamorphic recrystallization. In the coarse fraction 2–50 μm, the staircase pattern of the age spectrum to a maximum value of ∼107 Ma is interpreted to reflect the coexistence of partially reset detrital Variscan muscovite ($2M_1$), of diagenetic mica (1M) and of newly formed syn-kinematic mica ($2M_1$). Therefore, the late Cretaceous-Paleocene $^{40}Ar/^{39}Ar$ RAs and TGAs (64–67 Ma) are considered to be mixed ages.

The fraction 0.5–2 μm is slightly enriched in $2M_1$ polytype and provides younger and broadly similar RAs and TGAs that fall in the Middle Eocene (44–47 Ma). This suggests that the mechanisms of dissolution-recrystallization during the $D_1/M_1$ metamorphic event at ∼300°C were more efficient for this smaller size Wm population, leading to a significant isotopic resetting of the prekinematic Wm. Whether or not this resetting is complete will be further examined in the light of the data provided by the two smallest grain-size fractions of 0.5–0.2 μm and <0.2 μm. These fractions display the highest proportion of Wm and $2M_1$ polytype relative to 1M. They show similar age spectra that mainly differ by the amount of $^{39}$Ar recoil loss and both contain a small amount of $^{38}Ar_{(Cl)}$ that is lacking in the coarser fractions. This indicates that the fine-grained Wm grains were in equilibrium with the surrounding intergranular (syn-tectonic) fluid(s) when they (re)crystallized and suggests that the <0.5 μm $Wm_d$ may have behaved as open isotopic systems during the $D_1/M_1$ tectonometamorphic event. This is consistent with the fact that the peak metamorphic temperature reached during shearing was high enough to induce a complete resetting of Wm by volume diffusion, considering the diffusion parameters of Harrison et al. (2009), compatible with those of Kirschner et al. (1996) for fine-grained Wm. A modeling of the argon behavior based on these diffusion data (Ehlers et al., 2005) shows that reheating at 300°C for 5 Ma can induce a total loss of radiogenic argon in the $Wm_d$ of the Tizgarine unit with a grain size < 0.5 μm. Certainly this loss was enhanced by the dissolution-recrystallization processes that accompanied reheating during shearing (Villa et al., 2014).

Both RAs of these two fined-grained fractions are 38 ± 0.2 Ma (Table 4), with TGAs of 33.8 ± 0.1 Ma and 29.8 ± 0.2 Ma, respectively. Assuming that prekinematic (detrital) white mica experienced full resetting and that a single age population made of fully reset and newly formed white mica ($Wm_m$) is present in these fractions, the age variations can be viewed as recording a grain-size effect on the retention of radiogenic argon and on $^{39}$Ar recoil loss in the Wm crystallites. Since the recoil distance for the neutron reaction producing $^{39}$Ar is ∼0.162 μm (Onstott et al., 1995), $^{39}$Ar recoil loss can be expected to be significant in the two finer

grain-size fractions and higher in the fraction <0.2 μm which is in agreement with our data (Table 4). The amount of $^{39}$Ar recoil depends not only on the grain size but also on the distribution of the K atoms in the TOT structure of the crystallites and on their thickness (see Fitz-Díaz et al., 2016 for a review). Moreover, it is likely that radiogenic argon produced by the natural decay of $^{40}$ K in poorly retentive sites of the crystallites (surfaces, vacancies, dislocations) may have escaped in the intergranular space. Consequently, these two competing processes, leading to younger ages for fine-grained white micas complicate interpretation of RAS and TGAs. In some circumstances, TGAs fit regional geological constraints; in others, RAs appear to give a better estimate of the geological event to be dated.

Fitz-Díaz et al. (2016) proposed a method of correction of TGAs based on XRD data to consider the effect of illite crystallite thickness (ICT) on argon retention. This method can be applied to anchizonal-epizonal micas with thickness values between 10 and 50 nm, which is the range observed in the Wm fractions <0.5 μm of Tizgarine unit, showing a ratio length/thickness of the crystallites close to 10 (SEM and XRD measurements; see Figure S1). The ICTs calculated on oriented fractions 0.5–0.2 and <0.2 μm provide values of 22–26 nm and 8–15 nm, respectively (Table 4). The corrected ages (XCA) of the two finest fractions are reported in Table 4. The fraction 0.5–0.2 μm with a TGA of 33.8 ± 0.1 Ma yields a XCA of 36.8 ± 0.2 Ma, very close to its RA of 38.4 ± 0.1 Ma. The finest fraction with a TGA of 29.8 ± 0.2 Ma has an XCA of 34.4 ± 1.1 Ma, about 4 Ma younger than its RA. The XCAs of these two fractions are relatively consistent and about 10 Ma younger than the ages provided by the upper grain-size fraction of 0.5–2 μm. They can be interpreted as recording an equilibrium state and isotopic closure of syn-metamorphic $2M_1$ Wm in the TZ unit during the period of 37 to 34 Ma (Priabonian; late Eocene).

Whether these ages are crystallization or cooling ages can be assessed by comparing the theoretical closure temperature of these micas with that of peak metamorphism. We calculated the closure temperature of these fine-grained Wm using diffusion data of Harrison et al. (2009) and cooling rates in the range 10–50°C/Ma (Ehlers et al., 2005). This approach gives closure temperatures of 257–271°C and 237–250°C, respectively, for the two fractions, with an uncertainty of about 50°C due to the large uncertainty (10%) on the activation energy for argon diffusion in Wm (Harrison et al., 2009). Considering this uncertainty, these closure temperatures are slightly below or similar to the peak metamorphic temperature of ∼300°C during the $D_1/M_1$ event and could indicate that the ages of 37-34 Ma represent the end of $D_1/M_1$ (re)crystallization processes and the beginning of exhumation of Tizgarine unit. These ages are consistent with the $^{40}$Ar/$^{39}$Ar phengite age of 38 Ma recently reported for HP/LT rocks of the Alpujarride units in the Betic Cordilleras (Bessière et al., 2021).

The middle Eocene RA and TGA provided by the fraction 0.5–2 μm might indicate that the $D_1/M_1$ Alpine tectonometamorphic event began earlier, in agreement with Platt et al. (2005) for the Eastern Betic Cordilleras. In the Rif, this hypothesis can be discarded for the following reasons: (i) the 0.5–2 μm fraction still contains a large proportion of diagenetic 1M mica formed before the Alpine $D_1/M_1$ event; (ii) there is no evidence of $^{38}Ar_{(Cl)}$ exchange with the intergranular fluid(s) and of a full open behavior (resetting) of the detrital micas with a grain size > 0.5 μm; and (iii) a plot of TGA versus % $2M_1$ of the three fractions <2 μm (Haines & van der Pluijm, 2008) yields a negative slope that suggests that the fraction 0.5–2 μm contains more than one generation of $2M_1$ Wm (Figure S2).

### 5.2. The Age of the Postorogenic Extensional Detachment Tectonics

The XRD analysis of the Zaouia fault gouge (S17-21B) documents Chl, Qz, Ab, Kln, Wm as the main mineral components, with nearly constant proportions of Chl (31–36%) and Wm (24–29%) in the grain-size fractions < 2 μm and an increase of Kln (7–35%) toward the finest fraction (Tables 2 and 3). Remarkably, the increase of the 1M Wm polytype with decreasing grain size is compatible with the low-temperature conditions associated to brittle faulting (e.g., Aldega et al., 2019; Curzi et al., 2020; Haines & van der Pluijm, 2008; van der Pluijm et al., 2001).

Wm is the only K-rich mineral that produced radiogenic argon in this sample and only two age components are present, inherited $2M_1$ metamorphic Wm and 1M authigenic mica. $^{40}$Ar/$^{39}$Ar dating of the four fractions yields similar TGAs in the range 21-18.4 Ma for a proportion of $2M_1$ polytype relative to 1M between nearly 100% to 54%. Compared to the Tizgarine unit sample S17-02, the amount of $^{39}$Ar lost during irradiation by

recoil effect is quite important (12.0–32.6%, Table 4) and probably relates to the fact that numerous dislocations affected the crystallographic structure of the micas during faulting, thus favoring the development of new short pathways for the ejection of $^{39}$Ar during neutron irradiation. This may be the reason for the more irregular age spectra compared to those from TZ unit sample S17-02 (three out of four spectra showing hump-shaped patterns; Figure 10b), which may be related to a complex loss/redistribution of $^{39}$Ar in broken and recrystallized Wm of different grain size and polytype.

The age spectrum of the coarsest 2–50 μm fraction (94–100% of $2M_1$) displays no evidence of a pre-Alpine age component and provides a TGA of 21.0 ± 0.1 Ma that is consistent with the Early Miocene metamorphic ages commonly recovered from the Sebtide Complex (see Sections 1 and 2) and, particularly, by Ar-Ar biotite ages in the Filali unit at the immediate footwall of the Zaouia Fault (Michard et al., 2006). This age can be considered as the age of the older Wm end-member in the Zaouia fault gouge. In the three finer fractions (<2 μm), ages older than 21 Ma are recorded by individual steps on the age spectra (Figure 11a) and by RAs and XCAs (Table 4). As indicated above, the presence of an old detrital component can be discarded to explain these ages that are viewed mainly as the consequence of $^{39}$Ar recoil effects. Among these fractions, the finest grained (<0.2 μm) has a TGA of 18.4 ± 0.2 Ma, which represents an upper age limit for the brittle activity of the Zaouia fault in the upper crust. Figures 11b represents an attempt to correlate TGAs with the proportion of $2M_1$ mica polytype in the different fractions using IsoplotR software (Vermeesch, 2018). This plot yields an intercept age of 16.8 ± 0.8 Ma for the crystallization of 1M polytype and formation of the fault gouge at the contact between the Ghomaride and Sebtide Complexes. However, this late Burdigalian age must be treated with some caution since the representative data points are not widely dispersed along the regression line. Significantly, however, the Burdigalian age of the Zaouia Fault is consistent with the $^{40}$Ar/$^{39}$Ar illite dating of the extensional fault gouges cutting across the Lower Sebtides units of the Ceuta area (Münch et al., 2021, Figure 2a).

### 5.3. Implications at Regional Scale

Despite the limited number of geochronology samples, the new time-deformation history as reconstructed in this study conforms to a ca. 20 Ma long tectonic evolution (from the late Eocene to the early Miocene) that, framed within the regional tectonic and chronostratigraphic scenario of the Alboran Domain (Figure 12), provides a new reference frame for the Alpine evolution of the Western Mediterranean region. In particular, results of this study contribute to our understanding of the tectonism and timing of exhumation of the Alpujarride-Sebtide Complex of the Alboran Domain, with published models indicating either pre-Miocene syn-orogenic (Azañón & Crespo-Blanc, 2000; Azañón et al., 1998; Balanyá et al., 1997; Booth-Rea et al., 2005; Simancas & Campos, 1993; Tubía et al., 1992; Rossetti et al., 2005; Vergés & Fernàndez, 2012) or early Miocene late-to postorogenic (Platt & Vissers, 1989; Platt et al., 2013; Williams & Platt, 2018) scenarios.

The late Eocene (~37-34 Ma) ages in the TZ unit of the Upper Sebtides provide the first absolute time constraint for development of the Alpine $D_1/M_1$ orogenic fabric in the Alboran Domain of the Rif. This scenario is in line and supports the Eocene timing already proposed for the Betic counterpart (Augier et al., 2005; Bessière et al., 2021; Li & Massonne, 2018; Massonne, 2014; Platt et al., 2005). Significantly, the late Eocene timing for the Alpine $D_1/M_1$ event is also compatible with the tectonostratigraphic reconstruction of the Ghomaride-Malaguide complex, where the same time period for the Alpine orogenic event has been proposed (Chalouan et al., 2008; Lonergan, 1993; Serrano et al., 2006). The Alpine SW-verging $D_1/M_1$ shortening (present coordinates) documented in the TZ unit of the Upper Sebtides, together with the southward thrusting and imbrication of the Alpujarride Complex in the Sierra Alhamilla of the Betics (Williams & Platt, 2018), therefore constrain the orogenic process during construction of an Eocene, Africa-verging orogenic wedge, formed at the expenses of the Alpujarride-Sebtide and Ghomaride-Malaguide complexes. The Alpine thrusting then progressively involved the detached Mesozoic cover rocks of the Dorsale Calcaire during late Oligocene-early Miocene time (Vitale et al., 2015) (Figure 12).

The Alpine orogenic construction of the Western Mediterranean region as reconstructed in this study is consistent with the tectonometamorphic evolution of basement-involved thrusting and nappe stacking in the hinterland of the Apennine-Maghrebian chain (Figure 1), where similar late Eocene ages for the HP metamorphism (Eastern Kabylia: Bruguier et al., 2017; Calabria: Heymes et al., 2010; Rossetti et al., 2001, 2004; Schenk, 1980) and "Africa-verging" orogenic structures are reported (Calabria and Sicilia: Cirrincione

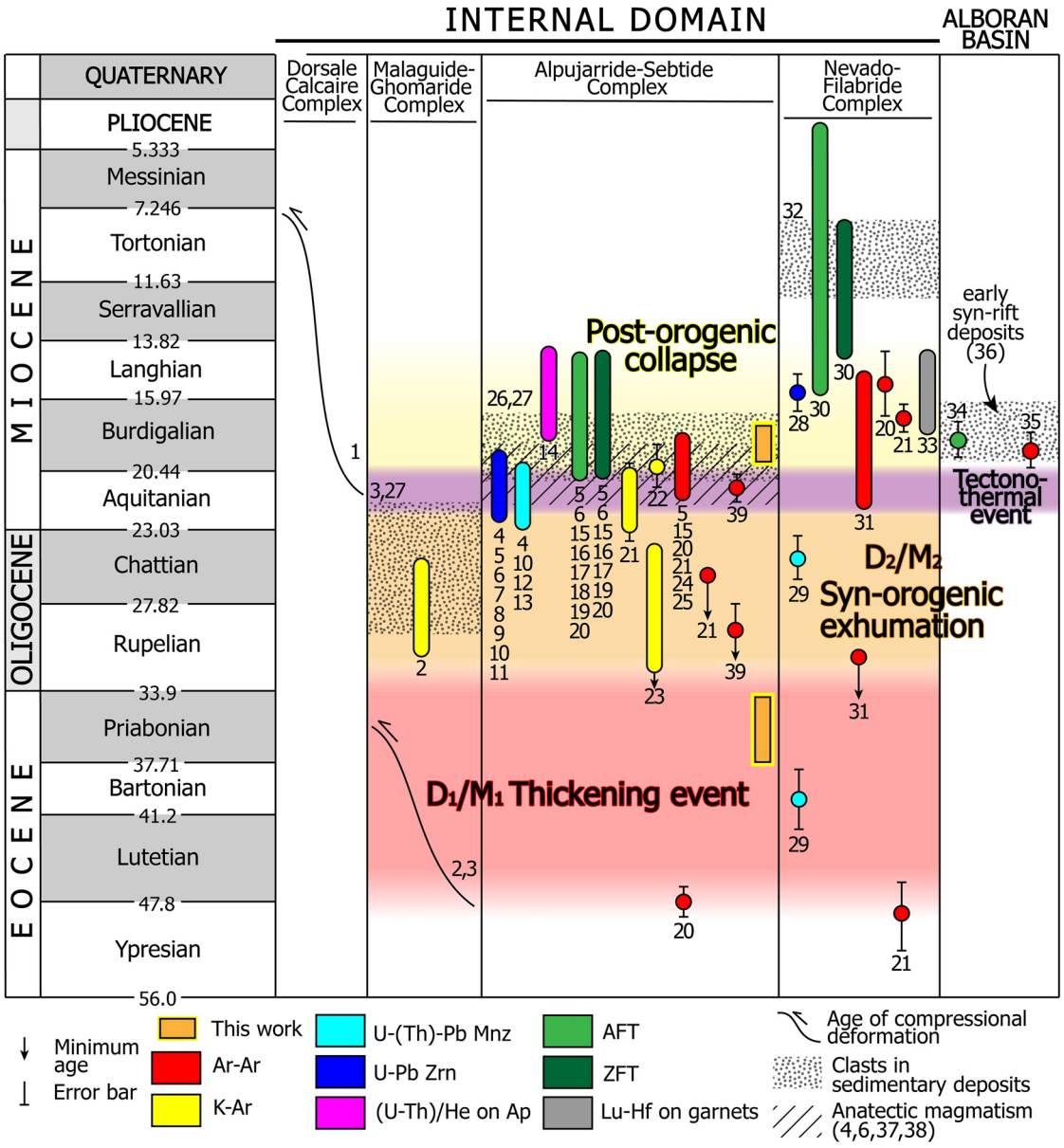


**Figure 12.** Tectonic and chronostratigraphic chart for the hinterland domain of the Betic-Rif orogen of the Western Mediterranean, with indication of the main Alpine tectonometamorphic stages as reconstructed in this study. List of references: 1, Vitale et al. (2015); 2, Chalouan and Michard (1990); 3, Lonergan (1993); 4, Rossetti et al. (2010, 2020); 5, Platt, Whitehouse, et al. (2003); 6, Esteban et al. (2007); 7, Esteban et al. (2011); 8, Platt and Whitehouse (1999); 9, Zeck and Williams (2001); 10, Homonnay et al. (2018); 11, Sánchez-Rodríguez and Gebauer (2000); 12, Janots et al. (2006); 13, Gueydan et al. (2015); 14, Romagny et al. (2014); 15, Platt, Argles, et al. (2003); 16, Esteban et al. (2004); 17, Azdimousa et al. (2014); 18, Sosson et al. (1998); 19, Andriessen and Zeck (1996); 20, Platt et al. (2005); 21, Monié et al. (1991); 22, Priem et al. (1979); 23, Michard et al. (2006); 24, Monié et al. (1994); 25, Frasca et al. (2016); 26, Lonergan and Mange-Rajetzky (1994); 27, Serrano et al. (2006); 28, López Sánchez-Vizcaíno et al. (2001); 29, Li and Massonne (2018); 30, Johnson et al. (1997); 31, Augier et al. (2005); 32, García-Dueñas et al. (1992); 33, Platt et al., (2006); 34, Hurford et al. (1999); 35, Platt et al. (1998) and Kelley and Platt (1999); 36, Comas et al. (1992); 37, Sánchez-Navas et al. (2014); 38, Rossetti et al. (2013); 39, Marrone et al. (2021).

et al., 2015; Dietrich, 1988; Rossetti et al., 2001; Vignaroli et al., 2008, 2012). This correlation allows to frame the Eocene $D_1/M_1$ orogenic construction along the Cenozoic convergence zone developed along the Apennine-Maghrebian subduction zone (e.g., Faccenna et al., 2004; Lacombe & Jolivet, 2005; Malusà et al., 2015; Rosenbaum et al., 2002; Williams & Platt, 2018).

Transition from shortening to extension in the Alboran Domain occurred in the early Miocene (Figure 12). Brittle postorogenic extensional tectonics is documented since the Burdigalian, as constrained by timing

of the extensional faulting in the hinterland of the Rif chain. The Burdigalian age is consistent with the low-temperature thermochronological results as available for the Alpujarride-Sebtide Complex as a whole, which document Burdigalian-Langhian ages (Andriessen & Zeck, 1996; Azdimousa et al., 2014; Esteban et al., 2004, 2007; Platt et al., 2003a, 2003b; Romagny et al., 2014; Sosson et al., 1998). This evidence shows that the Alboran Domain was exhumed to upper crustal conditions and thinned in the brittle crust at that time. Significantly, this age also overlaps in time with (a) that of the detachment style extension documented in the internal Betics (Mecina and the Filabres; Crespo-Blanc, 1995; Crespo-Blanc et al., 1994; García-Dueñas et al., 1992; Martínez-Martínez & Azañón, 1997; Martínez-Martínez et al., 2002; Williams & Platt, 2018), and (b) the formation of the syn-rift basins associated with the Alboran back-arc rifting (Bourgois et al., 1992; Chalouan et al., 1997; Comas et al., 1999; Do Couto et al., 2016; Soto & Platt, 1999).

Consequently, exhumation of the Alboran Domain in the ductile crust was almost complete by the early Miocene, as also documented by (a) the Alpujarride-derived clastic supply in the early Miocene deposits that unconformably cover the hinterland nappe stack in the Betics (Lonergan & Mange-Rajetzky, 1994; Serrano et al., 2006) (Figure 12) and (b) by the postmetamorphic nappe stacking as documented in the Betics prior to the Miocene rifting (Azañón & Crespo-Blanc, 2000). In this regard, the overall shapes of the retrogressive P-T paths as derived from the HP units of the Alpujarride-Sebtide Complex, document cooling during exhumation (Azañón et al., 1998; Bouybaouene et al., 1995; Marrone et al., 2021; Vidal et al., 1999). This indicates that, during regional exhumation, large portions of the Alpine, subduction-related metamorphic units during their way back to the surface escaped the early Miocene thermal overprint documented on the floor of the Alboran Basin (Platt et al., 1998; Soto & Platt, 1999). The different $D_1/M_1$ thermal signatures recorded by the tectonic slices forming the Alpujarride-Sebtide nappe stack of the Alboran Domain (Azañón & Crespo-Blanc, 2000; Azañón et al., 1998; Michard et al., 2006; Vidal et al., 1999) can be thus interpreted in terms of their different paleotectonic positions within the Alpine subduction channel prior to the Alboran extension: more external and shallowly located for the low-grade units (early exhumed; e.g., Lújár-Gador in the Betics, Tizgarine unit in the Rif), and more internal and deeper for the higher-grade ones (e.g., Salobreña, Herradura, and Adra, units in the Betics, Beni Mzala unit in the Rif). This reconstruction is therefore consistent with the idea that the major contribution to the exhumation history of the Alboran Domain occurred in a convergent plate setting, during crustal thickening and orogenic construction in the Eocene-Oligocene time span (syn-orogenic exhumation in Figure 12).

We therefore propose that transition from crustal shortening to extension in the hinterland (back-arc domain) of the Betic-Rif chain was controlled by the retreat of the western termination of the Apennine-Maghrebian subduction zone during the late Oligocene-early Miocene formation of the Alboran Basin (postorogenic extension in Figure 12). This scenario (see also Bessière et al., 2021; Bezada et al., 2013; Bokelmann et al., 2011; Booth-Rea et al., 2007; Faccenna et al., 2004; Frasca et al., 2015; Hidas et al., 2013; Jolivet et al., 2003; Lonergan & White, 1997; Malusà et al., 2015; Rossetti et al., 2013; Spakman & Wortel, 2004) is compatible with (a) crustal heating and elevation of the geothermal gradient in the thinned Alpine orogenic wedge in the hinterland during rollback of the delaminated lithosphere; (b) the outward progressive migration of the compressional fronts synchronously with the opening of the Alboran Basin; and (c) the allochthonous nature of the early structured Alboran Domain nappe stack within the Miocene external domains of the Betic-Rif chain.

## 6. Conclusions

The study of the lower-grade units exposed in the Alboran Domain of the internal Rif allow refinement of the Alpine orogenic and postorogenic evolution of the Western Mediterranean region. A 20 Ma long tectonic history is reconstructed that can be synthesized as follows:

1. A late Eocene (Priabonian, 37-34 Ma) age is documented for the Alpine $D_1/M_1$ thickening event in the Alboran Domain during formation of an Africa-verging (SW-directed, present coordinates) orogenic wedge
2. An Eocene age for the Alpine orogenic metamorphism must be considered for the geodynamic modeling of Western Mediterranean, consistently with the tectonometamorphic evolution of basement-involved thrusting in the orogenic hinterland of the Apennine-Maghrebian subduction

3. The postorogenic brittle extension is constrained during the Burdigalian (18-17 Ma), when the early formed orogen was thinned during formation of the Alboran Basin, in the back-arc domain of the Apennine-Maghrebian subduction

## Data Availability Statement

All data supporting the interpretations and conclusions of this study can be found in the manuscript text, figures, and the supporting information file and have been also placed in the online data repository OSF at https://osf.io/tyjuk/ (https://doi.org/10.17605/OSF.IO/TYJUK).

**Acknowledgments**
Moritz Schmeltz is thanked for sample preparation. The Grant to Department of Science, Roma Tre University (MIUR-Italy Dipartimenti di Eccellenza, ARTICOLO 958 1, COMMI 314-337 LEGGE 232/2016) is gratefully acknowledged. Figure 1a was produced with the GMT software package (Wessel et al., 2013). Constructive reviews and comments from J.-I. Soto, J. R. Williams and J. Wijbrans greatly contributed to improve the manuscript.

## References

Abd Elmola, A., Buatier, M., Monié, P., Labaume, P., Trap, P., & Charpentier, D. (2018). $^{40}Ar/^{39}Ar$ muscovite dating of thrust activity: A case study from the Axial Zone of the Pyrenees. *Tectonophysics*, *745*, 412–429. https://doi.org/10.1016/j.tecto.2018.09.004

Acosta-Vigil, A., Rubatto, D., Bartoli, O., Cesare, B., Meli, S., Pedrera, A., et al. (2014). Age of anatexis in the crustal footwall of the Ronda peridotites, S Spain. *Lithos*, *210*, 147–167. https://doi.org/10.1016/j.lithos.2014.08.018

Aldega, L., Viola, G., Casas-Sainz, A., Marcén, M., Román-Berdiel, T., & van der Lelij, R. (2019). Unraveling multiple thermo-tectonic events accommodated by crustal-scale faults in northern Iberia, Spain: Insights from K-Ar dating of clay gouges. *Tectonics*, *38*(10), 3629–3651. https://doi.org/10.1029/2019TC005585

Aldinucci, M., Gandin, A., & Sandrelli, F. (2008). The Mesozoic continental rifting in the Mediterranean area: Insights from the Verrucano tectofacies of southern Tuscany (Northern Apennines, Italy). *International Journal of Earth Sciences*, *97*(6), 1247–1269. https://doi.org/10.1007/s00531-007-0208-9

Álvarez-Valero, A. M., Jagoutz, O., Stanley, J., Manthei, C., Maz, A. E., Moukadiri, A., & Piasecki, A. (2014). Crustal attenuation as a tracer for the emplacement of the Beni Bousera ultramafic massif (Betico-Rifean belt). *Geological Society of America Bulletin*, *126*(11–12), 1614–1624. https://doi.org/10.1130/B31040.1

Andriessen, P. A. M., & Zeck, H. P. (1996). Fission-track constraints on timing of Alpine nappe emplacement and rates of cooling and exhumation, Torrox area, Betic Cordilleras, S. Spain. *Chemical Geology*, *131*(1–4), 199–206. https://doi.org/10.1016/0009-2541(95)00148-4

Andrieux, J., Fontbote, J. M., & Mattauer, M. (1971). Sur un modele explicatif de l'arc de Gibraltar. *Earth and Planetary Science Letters*, *12*(2), 191–198. https://doi.org/10.1016/0012-821X(71)90077-X

Argles, T. W., Platt, J. P., & Waters, D. J. (1999). Attenuation and excision of a crustal section during extensional exhumation: The Carratraca Massif, Betic Cordillera, southern Spain. *Journal of the Geological Society*, *156*(1), 149–162. https://doi.org/10.1144/gsjgs.156.1.0149

Augier, R., Agard, P., Monié, P., Jolivet, L., Robin, C., & Booth-Rea, G. (2005). Exhumation, doming and slab retreat in the Betic Cordillera (SE Spain): In situ $^{40}Ar/^{39}Ar$ ages and P-T-d-t paths for the Nevado-Filabride complex. *Journal of Metamorphic Geology*, *23*(5), 357–381. https://doi.org/10.1111/j.1525-1314.2005.00581.x

Azañón, J. M., & Crespo-Blanc, A. (2000). Exhumation during a continental collision inferred from the tectonometamorphic evolution of the Alpujarride Complex in the central Betics (Alboran Domain, SE Spain). *Tectonics*, *19*(3), 549–565. https://doi.org/10.1029/2000TC900005

Azañón, J. M., García-Dueñas, V., & Goffé, B. (1998). Exhumation of high-pressure metapelites and coeval crustal extension in the Alpujarride complex (Betic Cordillera). *Tectonophysics*, *285*(3–4), 231–252. https://doi.org/10.1016/S0040-1951(97)00273-4

Azdimousa, A., Bourgois, J., Poupeau, G., Vázquez, M., Asebriy, L., & Labrin, E. (2014). Fission track thermochronology of the Beni Bousera peridotite massif (Internal Rif, Morocco) and the exhumation of ultramafic rocks in the Gibraltar Arc. *Arabian Journal of Geosciences*, *7*(5), 1993–2005. https://doi.org/10.1007/s12517-013-0924-3

Balanyá, J. C., & García-Dueñas, V. (1988). El cabalgaminto cortical de Gibraltar y la tectónica de Béticas y Rif. In *Congreso geológico de España* (Vol. 2, pp. 35–44).

Balanyá, J. C., García-Dueñas, V., Azañón, J. M., & Sánchez-Gómez, M. (1997). Alternating contractional and extensional events in the Alpujarride nappes of the Alboran Domain (Betics, Gibraltar Arc). *Tectonics*, *16*(2), 226–238. https://doi.org/10.1029/96TC03871

Barich, A., Acosta-Vigil, A., Garrido, C. J., Cesare, B., Tajčmanová, L., & Bartoli, O. (2014). Microstructures and petrology of melt inclusions in the anatectic sequence of Jubrique (Betic Cordillera, S Spain): Implications for crustal anatexis. *Lithos*, *206*, 303–320. https://doi.org/10.1016/j.lithos.2014.08.003

Behr, W. M., & Platt, J. P. (2012). Kinematic and thermal evolution during two-stage exhumation of a Mediterranean subduction complex. *Tectonics*, *31*, TC4025. https://doi.org/10.1029/2012TC003121

Bessière, E., Jolivet, L., Augier, R., Scaillet, S., Précigout, J., Azañon, J. M., et al. (2021). Lateral variations of pressure-temperature evolution in non-cylindrical orogens and 3-D subduction dynamics: The Betic-Rif Cordillera example. *BSGF Earth Sciences Bulletin*, *192*, 8. https://doi.org/10.1051/bsgf/2021007

Bezada, M. J., Humphreys, E. D., Toomey, D. R., Harnafi, M., Dávila, J. M., & Gallart, J. (2013). Evidence for slab rollback in westernmost Mediterranean from improved upper mantle imaging. *Earth and Planetary Science Letters*, *368*, 51–60. https://doi.org/10.1016/j.epsl.2013.02.024

Bokelmann, G., Maufroy, E., Buontempo, L., Morales, J., & Barruol, G. (2011). Testing oceanic subduction and convective removal models for the Gibraltar arc: Seismological constraints from dispersion and anisotropy. *Tectonophysics*, *502*(1–2), 28–37. https://doi.org/10.1016/j.tecto.2010.08.004

Booth-Rea, G., Azanón, J. M., Martínez-Martínez, J. M., Vidal, O., & García-Dueñas, V. (2005). Contrasting structural and P-T evolution of tectonic units in the southeastern Betics: Key for understanding the exhumation of the Alboran Domain HP/LT crustal rocks (western Mediterranean). *Tectonics*, *24*, TC2009. https://doi.org/10.1029/2004TC001640

Booth-Rea, G., Ranero, C. R., Martínez-Martínez, J. M., & Grevemeyer, I. (2007). Crustal types and tertiary tectonic evolution of the Alborán sea, western Mediterranean. *Geochemistry, Geophysics, Geosystems*, *8*, Q10005. https://doi.org/10.1029/2007GC001639

Bourgois, J., Chauve, P., Magne, J., Monnot, J., Peyre, Y., Rigo, E., et al. (1972). La formation de Las Millanas. Série burdigalienne transgressive sur les zones internes des Cordillères bétiques occidentales (région d'Alozaina-Tolox, province de Malaga, Espagne). *Comptes Rendus de l'Académie des Sciences*, *275*, 169–172.

Bourgois, J., Mauffret, A., Ammar, A., & Demnati, A. (1992). Multichannel seismic data imaging of inversion tectonics of the Alboran Ridge (Western Mediterranean Sea). *Geo-Marine Letters*, *12*(2–3), 117–122. https://doi.org/10.1044/jshr.3506.1344

Bouybaouene, M. L., Goffé, B., & Michard, A. (1995). High-pressure, low-temperature metamorphism in the Sebtides nappes, northern Rif, Morocco. *Geogaceta*, *17*, 117–119.

Bouybaouene, M. L., Michard, A., & Goffé, B. (1998). High-pressure granulites on top of the Beni Bousera peridotites, Rif belt, Morocco: A record of an ancient thickened crust in the Alboran domain. *Bulletin de La Société Géologique de France*, *169*(2), 153–162.

Brown, M. (2010). Paired metamorphic belts revisited. *Gondwana Research*, *18*(1), 46–59. https://doi.org/10.1016/j.gr.2009.11.004

Bruguier, O., Bosch, D., Caby, R., Vitale-Brovarone, A., Fernandez, L., Hammor, D., et al. (2017). Age of UHP metamorphism in the Western Mediterranean: Insight from rutile and minute zircon inclusions in a diamond-bearing garnet megacryst (Edough Massif, NE Algeria). *Earth and Planetary Science Letters*, *474*, 215–225. https://doi.org/10.1016/j.epsl.2017.06.043

Carminati, E., Lustrino, M., & Doglioni, C. (2012). Geodynamic evolution of the central and western Mediterranean: Tectonics vs. igneous petrology constraints. *Tectonophysics*, *579*, 173–192. https://doi.org/10.1016/j.tecto.2012.01.026

Casciello, E., Fernàndez, M., Vergés, J., Cesarano, M., & Torne, M. (2015). The Alboran Domain in the Western Mediterranean evolution: The birth of a concept. *Bulletin de La Société Géologique de France*, *186*(4–5), 371–384. https://doi.org/10.2113/gssgfbull.186.4-5.371

Cathelineau, M., & Nieva, D. (1985). A chlorite solid solution geothermometer the Los Azufres (Mexico) geothermal system. *Contributions to Mineralogy and Petrology*, *91*(3), 235–244. https://doi.org/10.1007/BF00413350

Chalouan, A., & Michard, A. (1990). The Ghomarides nappes, Rif coastal range, Morocco: A variscan chip in the Alpine belt. *Tectonics*, *9*(6), 1565–1583. https://doi.org/10.1029/TC009i006p01565

Chalouan, A., & Michard, A. (2004). The Alpine Rif Belt (Morocco): A case of mountain building in a subduction-subduction-transform fault triple junction. *Pure and Applied Geophysics*, *161*, 489–519. https://doi.org/10.1007/s00024-003-2460-7

Chalouan, A., Michard, A., El Kadiri, K., Negro, F., de Lamotte, F., Soto, J.-I., & Saddiqi, O. (2008). The Rif Belt. In A. Michard, O. Saddiqi, A. Chalouan, & D. de Lamotte (Eds.), *Continental evolution: The geology of Morocco: Structure, stratigraphy, and tectonics of the Africa-Atlantic-Mediterranean Triple Junction* (pp. 203–302). Berlin, Heidelberg Springer. https://doi.org/10.1007/978-3-540-77076-3_5

Chalouan, A., Saji, R., Michard, A., & Bally, A. W. (1997). Neogene tectonic evolution of the southwestern Alboran Basin as inferred from seismic data off Morocco. *American Association of Petroleum Geologists Bulletin*, *81*(7), 1161–1184. https://doi.org/10.1306/522B4A0F-1727-11D7-8645000102C1865D

Cirrincione, R., Fazio, E., Fiannacca, P., Ortolano, G., Pezzino, A., & Punturo, R. (2015). The Calabria-Peloritani Orogen, a composite terrane in Central Mediterranean; its overall architecture and geodynamic significance for a pre-Alpine scenario around the Tethyan basin. *Periodico di Mineralogia*, *84*(3B), 701–749.

Clauer, N. (2013). The K-Ar and $^{40}Ar/^{39}Ar$ methods revisited for dating fine-grained K-bearing clay minerals. *Chemical Geology*, *354*, 163–185. https://doi.org/10.1016/j.chemgeo.2013.05.030

Comas, M. C., García-Dueñas, V., & Jurado, M. J. (1992). Neogene tectonic evolution of the Alboran Sea from MCS data. *Geo-Marine Letters*, *12*(2–3), 157–164. https://doi.org/10.1007/bf02084927

Comas, M. C., Platt, J. P., Soto, J.-I., & Watts, A. B. (1999). The origin and tectonic history of the Alboran Basin: Insights from Leg 161 results. *Proceedings of the Ocean Drilling Program: Scientific Results*, *161*, 555–580. https://doi.org/10.2973/odp.proc.sr.161.262.1999

Crespo-Blanc, A. (1995). Interference pattern of extensional fault systems: A case study of the Miocene rifting of the Alboran basement (North of Sierra Nevada, Betic Chain). *Journal of Structural Geology*, *17*(11), 1559–1569. https://doi.org/10.1016/0191-8141(95)E0044-D

Crespo-Blanc, A., Orozco, M., & García-Dueñas, V. (1994). Extension versus compression during the Miocene tectonic evolution of the Betic chain. Late folding of normal fault systems. *Tectonics*, *13*(1), 78–88. https://doi.org/10.1029/93TC02231

Curzi, M., Aldega, L., Bernasconi, S. M., Berra, F., Billi, A., Boschi, C., et al. (2020). Architecture and evolution of an extensionally-inverted thrust (Mt. Tancia Thrust, Central Apennines): Geological, structural, geochemical, and K–Ar geochronological constraints. *Journal of Structural Geology*, *136*, 104059. https://doi.org/10.1016/j.jsg.2020.104059

Dalla Torre, M., Stern, W. B., & Frey, M. (1994). Determination of white K-mica polytype ratios: Comparison of different XRD methods. *Clay Minerals*, *29*(5), 717–726. https://doi.org/10.1017/S0009855800028223

Daudet, M., Mouthereau, F., Brichau, S., Crespo-Blanc, A., Gautheron, C., & Angrand, P. (2020). Tectono-stratigraphic and thermal evolution of the western Betic flysch: Implications for the geodynamics of South Iberian margin and Alboran Domain. *Tectonics*, *39*, e2020TC006093. https://doi.org/10.1029/2020TC006093

Dewey, J. F. (1988). Extensional collapse of orogens. *Tectonics*, *7*(6), 1123–1139. https://doi.org/10.1029/TC007i006p01123

Dewey, J. F., Helman, M. L., Knott, S. D., Turco, E., & Hutton, D. H. W. (1989). Kinematics of the western Mediterranean. *Geological Society, London, Special Publications*, *45*(1), 265–283. https://doi.org/10.1144/GSL.SP.1989.045.01.15

Didon, J., Durand-Delga, M., & Kornprobst, J. (1973). Homologies géologiques entre les deux rives du détroit de Gibraltar. *Bulletin de la Societe Geologique de France*, *7*(2), 77–105. https://doi.org/10.2113/gssgfbull.S7-XV.2.77

Dietrich, D. (1988). Sense of overthrust shear in the Alpine nappes of Calabria (southern Italy). *Journal of Structural Geology*, *10*(4), 373–381. https://doi.org/10.1016/0191-8141(88)90015-6

Díez, J. B., Broutin, J., & Ferrer, J. (2005). Difficulties encountered in defining the Permian–Triassic boundary in Buntsandstein facies of the western Peritethyan domain based on palynological data. *Palaeogeography, Palaeoclimatology, Palaeoecology*, *229*(1–2), 40–53. https://doi.org/10.1016/j.palaeo.2005.06.029

Do Couto, D., Gorini, C., Jolivet, L., Lebret, N., Augier, R., Gumiaux, C., et al. (2016). Tectonic and stratigraphic evolution of the Western Alboran Sea Basin in the last 25 Myrs. *Tectonophysics*, *677*, 280–311. https://doi.org/10.1016/j.tecto.2016.03.020

Doglioni, C., Gueguen, E., Sàbat, F., & Fernandez, M. (1997). The Western Mediterranean extensional basins and the Alpine orogen. *Terra Nova*, *9*(3), 109–112. https://doi.org/10.1046/j.1365-3121.1997.d01-18.x

Dong, H., Hall, C. M., Peacor, D. R., & Halliday, A. N. (1995). Mechanisms of argon retention in clays revealed by laser $^{40}Ar$-$^{39}Ar$ dating. *Science*, *267*(5196), 355–359. https://doi.org/10.1126/science.267.5196.355

Durand Delga, M., & Kornprobst, J. (1963). Esquisse géologique de la région de Ceuta (Maroc). *Bulletin de la Societe Geologique de France*, *7*(7), 1049–1057. https://doi.org/10.2113/gssgfbull.s7-v.7.1049

Ehlers, T. A., Chaudhri, T., Kumar, S., Fuller, C. W., Willett, S. D., Ketcham, R. A., et al. (2005). Computational tools for low-temperature thermochronometer interpretation. *Reviews in Mineralogy and Geochemistry*, *58*(1), 589–622. https://doi.org/10.2138/rmg.2005.58.22

El Kadiri, K., Linares, A., & Oloriz, F. (1992). La Dorsale calcaire rifaine (Maroc septentrional): Evolution stratigraphique et géodynamique durant le Jurassique-Crétacé. *Notes et mémoires du Service géologique*, *366*, 217–265.

El Maz, A., & Guiraud, M. (2001). Paragenese a faible variance dans les metapelites de la serie de Filali (Rif interne marocain): Description, interpretation et consequence geodynamique. *Bulletin de la Societe Geologique de France*, *4*, 469–485. https://doi.org/10.2113/172.4.469

Esteban, J. J., Cuevas, J., Tubía, J. M., Liati, A., Seward, D., & Gebauer, D. (2007). Timing and origin of zircon-bearing chlorite schists in the Ronda peridotites (Betic Cordilleras, Southern Spain). *Lithos*, *99*(1–2), 121–135. https://doi.org/10.1016/j.lithos.2007.06.006

Esteban, J. J., Cuevas, J., Tubía, J. M., Sergeev, S., & Larionov, A. (2011). A revised Aquitanian age for the emplacement of the Ronda peridotites (Betic Cordilleras, southern Spain). *Geological Magazine*, *148*(1), 183–187. https://doi.org/10.1017/S0016756810000737

Esteban, J. J., Sánchez-Rodríguez, L., Seward, D., Cuevas, J., & Tubía, J. M. (2004). The late thermal history of the Ronda area, southern Spain. *Tectonophysics*, *389*(1–2), 81–92. https://doi.org/10.1016/j.tecto.2004.07.050

Faccenna, C., Becker, T. W., Lucente, F. P., Jolivet, L., & Rossetti, F. (2001). History of subduction and back-arc extension in the central Mediterranean. *Geophysical Journal International*, *145*(3), 809–820. https://doi.org/10.1046/j.0956-540X.2001.01435.x

Faccenna, C., Piromallo, C., Crespo-Blanc, A., Jolivet, L., & Rossetti, F. (2004). Lateral slab deformation and the origin of the western Mediterranean arcs. *Tectonics*, *23*, TC1012. https://doi.org/10.1029/2002TC001488

Fallot, P. (1937). Essai sur la géologie du Rif Septentrional. *Notes et Mémoires du Service Géologique de Maroc*, *40*, 1–538.

Fitz-Díaz, E., Hall, C. M., & van der Pluijm, B. A. (2016). XRD-based $^{40}Ar/^{39}Ar$ age correction for fine-grained illite, with application to folded carbonates in the Monterrey Salient (northern Mexico). *Geochimica et Cosmochimica Acta*, *181*, 201–216. https://doi.org/10.1016/j.gca.2016.02.004

Frasca, G., Gueydan, F., & Brun, J. P. (2015). Structural record of Lower Miocene westward motion of the Alboran Domain in the Western Betics, Spain. *Tectonophysics*, *657*, 1–20. https://doi.org/10.1016/j.tecto.2015.05.017

Frasca, G., Gueydan, F., Brun, J. P., & Monié, P. (2016). Deformation mechanisms in a continental rift up to mantle exhumation. Field evidence from the western Betics, Spain. *Marine and Petroleum Geology*, *76*, 310–328. https://doi.org/10.1016/j.marpetgeo.2016.04.020

Frasca, G., Gueydan, F., Poujol, M., Brun, J. P., Parat, F., Monié, P., et al. (2017). Fast switch from extensional exhumation to thrusting of the Ronda Peridotites (South Spain). *Terra Nova*, *29*(2), 117–126. https://doi.org/10.1111/ter.12255

García-Casco, A., & Torres-Roldán, R. L. (1999). Natural metastable reactions involving garnet, staurolite and cordierite: Implications for petrogenetic grids and the extensional collapse of the Betic-Rif Belt. *Contributions to Mineralogy and Petrology*, *136*, 131–153. https://doi.org/10.1007/s004100050528

García-Dueñas, V., Balanyá, J. C., & Martínez-Martínez, J. M. (1992). Miocene extensional detachments in the outcropping basement of the northern Alboran Basin (Betics) and their tectonic implications. *Geo-Marine Letters*, *12*(2–3), 88–95. https://doi.org/10.1007/BF02084917

Garrido, C. J., Gueydan, F., Booth-Rea, G., Precigout, J., Hidas, K., Padrón-Navarta, J. A., & Marchesi, C. (2011). Garnet lherzolite and garnet-spinel mylonite in the Ronda peridotite: Vestiges of Oligocene backarc mantle lithospheric extension in the western Mediterranean. *Geology*, *39*(10), 927–930. https://doi.org/10.1130/G31760.1

Goffé, B., Azañón, J. M., Bouybaouene, M. L., & Jullien, M. (1996). Metamorphic cookeite in Alpine metapelites from Rif, northern Morocco, and the Betic Chain, southern Spain. *European Journal of Mineralogy-Ohne Beihefte*, *8*(2), 335–348. https://doi.org/10.1127/ejm/8/2/0335

Gómez-Pugnaire, M. T., Nieto, F., Abad, I., Velilla, N., Garrido, C. J., Acosta-Vigil, A., et al. (2019). Alpine Metamorphism in the Betic Internal Zones. In *The geology of Iberia: A geodynamic approach* (pp. 519–544). Springer. https://doi.org/10.1007/978-3-030-11295-0_13

Guerrera, F., Martín-Martín, M., & Tramontana, M. (2019). Evolutionary geological models of the central-western peri-Mediterranean chains: A review. *International Geology Review*, *63*, 1–86. https://doi.org/10.1080/00206814.2019.1706056

Gueydan, F., Mazzotti, S., Tiberi, C., Cavin, R., & Villaseñor, A. (2019). Western Mediterranean subcontinental mantle emplacement by continental margin obduction. *Tectonics*, *38*, 2142–2157. https://doi.org/10.1029/2018TC005058

Gueydan, F., Pitra, P., Afiri, A., Poujol, M., Essaifi, A., & Paquette, J. L. (2015). Oligo-Miocene thinning of the Beni Bousera peridotites and their Variscan crustal host rocks, Internal Rif, Morocco. *Tectonics*, *34*, 1244–1268. https://doi.org/10.1002/2014TC003769

Haines, S. H., & van der Pluijm, B. A. (2008). Clay quantification and Ar–Ar dating of synthetic and natural gouge: Application to the Miocene Sierra Mazatán detachment fault, Sonora, Mexico. *Journal of Structural Geology*, *30*(4), 525–538. https://doi.org/10.1016/j.jsg.2007.11.012

Haissen, F., Garcia-Casco, A., Torres-Roldan, R., & Aghzer, A. (2004). Decompression reactions and P–T conditions in high-pressure granulites from Casares-Los Reales units of the Betic-Rif belt (S Spain and N Morocco). *Journal of African Earth Sciences*, *39*(3–5), 375–383. https://doi.org/10.1016/j.jafrearsci.2004.07.030

Handy, M. R., Schmid, S. M., Bousquet, R., Kissling, E., & Bernoulli, D. (2010). Reconciling plate-tectonic reconstructions of Alpine Tethys with the geological–geophysical record of spreading and subduction in the Alps. *Earth-Science Reviews*, *102*(3–4), 121–158. https://doi.org/10.1016/j.earscirev.2010.06.002

Harrison, T. M., Célérier, J., Aikman, A. B., Hermann, J., & Heizler, M. T. (2009). Diffusion of $^{40}Ar$ in muscovite. *Geochimica et Cosmochimica Acta*, *73*(4), 1039–1051. https://doi.org/10.1016/j.gca.2008.09.038

Heymes, T., Monié, P., Arnaud, N., Pêcher, A., Bouillin, J. P., & Compagnoni, R. (2010). Alpine tectonics in the Calabrian-Peloritan belt (southern Italy): New $^{40}Ar/^{39}Ar$ data in the Aspromonte Massif area. *Lithos*, *114*(3–4), 451–472. https://doi.org/10.1016/j.lithos.2009.10.011

Hidas, K., Booth-Rea, G., Garrido, C. J., Martínez-Martínez, J. M., Padrón-Navarta, J. A., Konc, Z., et al. (2013). Backarc basin inversion and subcontinental mantle emplacement in the crust: Kilometer-scale folding and shearing at the base of the proto-Alborán lithospheric mantle (Betic Cordillera, southern Spain). *Journal of the Geological Society*, *170*(1), 47–55. https://doi.org/10.1144/jgs2011-151

Homonnay, E., Corsini, M., Lardeaux, J. M., Romagny, A., Münch, P., Bosch, D., et al. (2018). Miocene crustal extension following thrust tectonic in the Lower Sebtides units (internal Rif, Ceuta Peninsula, Spain): Implication for the geodynamic evolution of the Alboran domain. *Tectonophysics*, *722*, 507–535. https://doi.org/10.1016/j.tecto.2017.11.028

Horvath, F., Stegena, L., & Berckhemer, H. (1981). Models of Mediterranean back-arc basin formation. *Philosophical Transactions of the Royal Society of London—Series A: Mathematical and Physical Sciences*, *300*, 383–402. https://doi.org/10.1098/rsta.1981.0071

Hurford, A. J., Platt, J. P., & Carter, A. (1999). Fission-track analysis of samples from the Alboran sea basement. In *Proceedings of the Ocean Drilling Program: Scientific Results* (Vol. 161, p. 295). The Program.

Janots, E., Negro, F., Brunet, F., Goffé, B., Engi, M., & Bouybaouene, M. L. (2006). Evolution of the REE mineralogy in HP-LT metapelites of the Sebtide complex, Rif, Morocco: Monazite stability and geochronology. *Lithos*, *87*(3–4), 214–234. https://doi.org/10.1016/j.lithos.2005.06.008

Johnson, C., Harbury, N., & Hurford, A. J. (1997). The role of extension in the Miocene denudation of the Nevado-Filábride Complex, Betic Cordillera (SE Spain). *Tectonics*, *16*(2), 189–204. https://doi.org/10.1029/96TC03289

Jolivet, L., Augier, R., Faccenna, C., Negro, F., Rimmele, G., Agard, P., et al. (2008). Subduction, convergence and the mode of backarc extension in the Mediterranean region. *Bulletin de la Societe Geologique de France*, *179*(6), 525–550. https://doi.org/10.2113/gssgfbull.179.6.525

Jolivet, L., & Brun, J. P. (2010). Cenozoic geodynamic evolution of the Aegean. *International Journal of Earth Sciences*, *99*(1), 109–138. https://doi.org/10.1007/s00531-008-0366-4

Jolivet, L., & Faccenna, C. (2000). Mediterranean extension and the Africa-Eurasia collision. *Tectonics*, *19*(6), 1095–1106. https://doi.org/10.1029/2000TC900018

Jolivet, L., Faccenna, C., Goffé, B., Burov, E., & Agard, P. (2003). Subduction tectonics and exhumation of high-pressure metamorphic rocks in the Mediterranean orogens. *American Journal of Science*, *303*(5), 353–409. https://doi.org/10.2475/ajs.303.5.353

Jolivet, L., Faccenna, C., Goffé, B., Mattei, M., Rossetti, F., Brunet, C., et al. (1998). Midcrustal shear zones in postorogenic extension: Example from the northern Tyrrhenian Sea. *Journal of Geophysical Research: Solid Earth*, *103*(B6), 12123–12160. https://doi.org/10.1029/97JB03616

Jolivet, L., Faccenna, C., Huet, B., Labrousse, L., Le Pourhiet, L., Lacombe, O., et al. (2013). Aegean tectonics: Strain localisation, slab tearing and trench retreat. *Tectonophysics*, *597*, 1–33. https://doi.org/10.1016/j.tecto.2012.06.011

Kelley, S. P., & Platt, J. P. (1999). 22. Ar-Ar dating of biotite and muscovite from Alboran basement samples, site 9761. In *Proceedings of the Ocean Drilling Program: Scientific Results* (Vol. 161, p. 301). The Program.

Kirchner, K. L., Behr, W. M., Loewy, S., & Stockli, D. F. (2016). Early Miocene subduction in the western Mediterranean: Constraints from Rb-Sr multimineral isochron geochronology. *Geochemistry, Geophysics, Geosystems*, *17*, 1842–1860. https://doi.org/10.1002/2015GC006208

Kirschner, D. L., Cosca, M. A., Masson, H., & Hunziker, J. C. (1996). Staircase $^{40}Ar/^{39}Ar$ spectra of fine-grained white mica: Timing and duration of deformation and empirical constraints on argon diffusion. *Geology*, *24*(8), 747–750. https://doi.org/10.1130/00917613(1996)024<0747:SAASOF>2.3.CO;2

Kornprobst, J. (1974). *Contribution à l'etude petrographique et structurale de la zone interne du Rif (Maroc septentrional); petrography and structure of the Rif inner area, northern Morocco* (Vol. 251, p. 256), Notes et Mémoires du Service Géologique.

Kornprobst, J., & Durand-Delga, M. (1985). Cartes géologiques du Rif 1: 50000, (feuilles de Sebta). Notes et Mémoires du Service géologique du Maroc.

Lacombe, O., & Jolivet, L. (2005). Structural and kinematic relationships between Corsica and the Pyrenees-Provence domain at the time of the Pyrenean orogeny. *Tectonics*, *24*, TC1003. https://doi.org/10.1029/2004TC001673

Law, R. D. (2014). Deformation thermometry based on quartz c-axis fabrics and recrystallization microstructures: A review. *Journal of Structural Geology*, *66*, 129–161. https://doi.org/10.1016/j.jsg.2014.05.023

Leprêtre, R., de Lamotte, D. F., Combier, V., Gimeno-Vives, O., Mohn, G., & Eschard, R. (2018). The Tell-Rif orogenic system (Morocco, Algeria, Tunisia) and the structural heritage of the southern Tethys margin. *Bulletin de la Societe Geologique de France*, *189*(2), 10. https://doi.org/10.1051/bsgf/2018009

Li, B., & Massonne, H. J. (2018). Two Tertiary metamorphic events recognized in high-pressure metapelites of the Nevado-Filábride Complex (Betic Cordillera, S Spain). *Journal of Metamorphic Geology*, *36*(5), 603–630. https://doi.org/10.1111/jmg.12312

Linol, B., Bercovici, A., Bourquin, S., Diez, J. B., López-Gómez, J., Broutin, J., et al. (2009). Late Permian to Middle Triassic correlations and palaeogeographical reconstructions in south-western European basins: New sedimentological data from Minorca (Balearic Islands, Spain). *Sedimentary Geology*, *220*(1–2), 77–94. https://doi.org/10.1016/j.sedgeo.2009.06.003

Lister, G. S., & Baldwin, S. L. (1993). Plutonism and the origin of metamorphic core complexes. *Geology*, *21*(7), 607–610. https://doi.org/10.1130/0091-7613(1993)021<0607:PATOOM>2.3.CO;2

Lonergan, L. (1993). Timing and kinematics of deformation in the Malaguide Complex, internal zone of the Betic Cordillera, southeast Spain. *Tectonics*, *12*(2), 460–476. https://doi.org/10.1029/92TC02507

Lonergan, L., & Mange-Rajetzky, M. A. (1994). Evidence for Internal Zone unroofing from foreland basin sediments, Betic Cordillera, SE Spain. *Journal of the Geological Society*, *151*, 515–529. https://doi.org/10.1144/gsjgs.151.3.0515

Lonergan, L., & White, N. (1997). Origin of the Betic-Rif mountain belt. *Tectonics*, *16*(3), 504–522. https://doi.org/10.1029/96TC03937

López-Gómez, J., & Arche, A. (1993). Sequence stratigraphic analysis and paleogeographic interpretation of the Buntsandstein and Muschelkalk facies (Permo-Triassic) in the SE Iberian Range, E Spain. *Palaeogeography, Palaeoclimatology, Palaeoecology*, *103*(3–4), 179–201. https://doi.org/10.1016/0031-0182(93)90142-6

López Sánchez-Vizcaíno, V. L., Rubatto, D., Gómez-Pugnaire, M. T., Trommsdorff, V., & Müntener, O. (2001). Middle Miocene high-pressure metamorphism and fast exhumation of the Nevado-Filábride Complex, SE Spain. *Terra Nova*, *13*(5), 327–332. https://doi.org/10.1046/j.1365-3121.2001.00354.x

Maaté, A. (1996). *Stratigraphy and paleogeographic evolution of the Ghomarides Domain (Internal Rif, Morocco).* Ph.D. Thesis. (pp. 1–397). Universidad de Granada.

Malinverno, A., & Ryan, W. B. F. (1986). Extension in the Tyrrhenian Sea and shortening in the Apennines as result of arc migration driven by sinking of the lithosphere. *Tectonics*, *5*(2), 227–245. https://doi.org/10.1029/tc005i002p00227

Malusà, M. G., Faccenna, C., Baldwin, S. L., Fitzgerald, P. G., Rossetti, F., Danisik, M., et al. (2015). Contrasting styles of (U)HP rock exhumation along the Cenozoic Adria-Europe plate boundary (Western Alps, Calabria, Corsica). *Geochemistry, Geophysics, Geosystems*, *16*, 1786–1824. https://doi.org/10.1002/2015GC005767

Marrone, S., Monié, P., Rossetti, F., Lucci, F., Theye, T., Bouybaouene, M. L., & Zaghloul, M. N. (2021). The Pressure-Temperature-time-deformation history of the Beni Mzala unit (Upper Sebtides, Rif belt, Morocco): Refining the Alpine tectono-metamorphic evolution of the Alboran Domain of the Western Mediterranean. *Journal of Metamorphic Geology*, *39*(5), 591–615. https://doi.org/10.1111/jmg.12587

Martín-Algarra, A., Andreo, B., Balanyá, J. C., Estévez, A., López-Garrido, A. C., O'Dogherty, L., & García-Dueñas, V. (2004). Unidades Frontales de las zonas Internas. Geología de España, Chap. 4. Cordillera Bética y Baleares. Sociedad Geológica de España, Instituto Geológico y Minero de España, Madrid, pp. 396–401. https://doi.org/10.1086/597365

Martín-Algarra, A., Messina, A., Perrone, V., Russo, S., Maate, A., & Martín-Martín, M. (2000). A lost realm in the internal domains of the Betic-Rif orogen (Spain and Morocco): Evidence from conglomerates and consequences for Alpine geodynamic evolution. *The Journal of Geology*, *108*(4), 447–467. https://doi.org/10.1086/314410

Martínez, J. C., Dristas, J. A., Massonne, H. J., & Theye, T. (2010). A hydrothermal clay mineral assemblage at the Late Proterozoic unconformity in the Buenos Aires Complex-La Tinta Formation, Barker area, Tandilia Ranges (Argentina). *Clay Minerals*, *45*(2), 209–224. https://doi.org/10.1180/claymin.2010.045.2.209

Martínez-Martínez, J. M., & Azañón, J. M. (1997). Mode of extensional tectonics in the southeastern Betics (SE Spain): Implications for the tectonic evolution of the peri-Alborán orogenic system. *Tectonics*, *16*(2), 205–225. https://doi.org/10.1029/97TC00157

Martínez-Martínez, J. M., Soto, J.-I., & Balanyá, J. C. (2002). Orthogonal folding of extensional detachments: Structure and origin of the Sierra Nevada elongated dome (Betics, SE Spain). *Tectonics*, *21*(3), 1012. https://doi.org/10.1029/2001TC001283

Massonne, H. J. (2014). Wealth of P-T-t information in medium-high grade metapelites: Example from the Jubrique Unit of the Betic Cordillera, S Spain. *Lithos*, *208*, 137–157. https://doi.org/10.1016/j.lithos.2014.08.027

Mattauer, M. (1960). *Nouvelles données sur la "Dorsale calcaire" du Rif (Maroc).-C. r* (Vol. 250, pp. 374–376). Acad. Sci.
Mazzoli, S., & Martín-Algarra, A. (2011). Deformation partitioning during transpressional emplacement of a 'mantle extrusion wedge': The Ronda peridotites, western Betic Cordillera, Spain. *Journal of the Geological Society*, *168*(2), 373–382. https://doi.org/10.1144/0016-76492010-126
Mazzoli, S., Martín-Algarra, A., Reddy, S. M., Sánchez-Vizcaíno, V. L., Fedele, L., & Noviello, A. (2013). The evolution of the footwall to the Ronda subcontinental mantle peridotites: Insights from the Nieves unit (western Betic Cordillera). *Journal of the Geological Society*, *170*(3), 385–402. https://doi.org/10.1144/jgs2012-105
Melchiorre, M., Álvarez-Valero, A. M., Vergés, J., Fernàndez, M., Belousova, E. A., El Maz, A., & Moukadiri, A. (2017). In situ U-Pb zircon geochronology on metapelitic granulites of Beni Bousera (Betic-Rif system, N Morocco). *Special Paper of the Geological Society of America*, *526*(8), 151–171. https://doi.org/10.1130/2017.2526(08)
Michard, A., Goffé, B., Bouybaouene, M. L., & Saddiqi, O. (1997). Late Hercynian-Mesozoic thinning in the Alboran domain: Metamorphic data from the northern Rif, Morocco. *Terra Nova*, *9*(4), 171–174. https://doi.org/10.1046/j.1365-3121.1997.d01-24.x
Michard, A., Negro, F., Saddiqi, O., Bouybaouene, M. L., Chalouan, A., Montigny, R., & Goffé, B. (2006). Pressure-temperature-time constraints on the Maghrebide mountain building: Evidence from the Rif-Betic transect (Morocco, Spain), Algerian correlations, and geodynamic implications. *Comptes Rendus Geoscience*, *338*(1–2), 92–114. https://doi.org/10.1016/j.crte.2005.11.011
Molli, G., & Malavieille, J. (2011). Orogenic processes and the Corsica/Apennines geodynamic evolution: Insights from Taiwan. *International Journal of Earth Sciences*, *100*(5), 1207–1224. https://doi.org/10.1007/s00531-010-0598-y
Monié, P., Galindo-Zaldivar, J., Lodeiro, F. G., Goffé, B., & Jabaloy, A. (1991). $^{40}Ar/^{39}Ar$ geochronology of Alpine tectonism in the Betic Cordilleras (southern Spain). *Journal of the Geological Society*, *148*(2), 289–297. https://doi.org/10.1144/gsjgs.148.2.0289
Monié, P., Torres-Roldán, R. L., & García-Casco, A. (1994). Cooling and exhumation of the Western Betic Cordilleras, $^{40}Ar/^{39}Ar$ thermochronological constraints on a collapsed terrane. *Tectonophysics*, *238*(1–4), 353–379. https://doi.org/10.1016/0040-1951(94)90064-7
Montel, J. M., Kornprobst, J., & Vielzeuf, D. (2000). Preservation of old U-Th-Pb ages in shielded monazite: Example from the Beni Bousera Hercynian kinzigites (Morocco). *Journal of Metamorphic Geology*, *18*(3), 335–342. https://doi.org/10.1046/j.1525-1314.2000.00261.x
Münch, P., Caillaud, J., Monié, P., Grauby, O., Corsini, M., Ricci, J., et al. (2021). Direct dating of brittle extensional deformation contemporaneous of Neogene exhumation of the internal zones of the Rif Chain. *Tectonophysics*, *807*, 228800. https://doi.org/10.1016/j.tecto.2021.228800
Negro, F., Beyssac, O., Goffé, B., Saddiqi, O., & Bouybaouène, M. L. (2006). Thermal structure of the Alboran Domain in the Rif (northern Morocco) and the Western Betics (southern Spain). Constraints from Raman spectroscopy of carbonaceous material. *Journal of Metamorphic Geology*, *24*(4), 309–327. https://doi.org/10.1111/j.1525-1314.2006.00639.x
Nold, M., Uttinger, J., & Wildi, W. (1981). Géologie de la dorsale calcaire entre Tetouan et Assifane (Rif interne, Maroc). *Notes et Mémoire du Service géologique du Maroc*, *300*, 233.
Onstott, T. C., Miller, M. L., Ewing, R. C., Arnold, G. W., & Walsh, D. S. (1995). Recoil refinements: Implications for the $^{40}Ar/^{39}Ar$ dating technique. *Geochimica et Cosmochimica Acta*, *59*(9), 1821–1834. https://doi.org/10.1016/0016-7037(95)00085-E
Passchier, C. W., & Trouw, R. A. J. (2010). *Microtectonics* (2nd ed.). Springer.
Pedrera, A., Ruiz-Constán, A., García-Senz, J., Azor, A., Marín-Lechado, C., Ayala, C., et al. (2020). Evolution of the South-Iberian paleomargin: From hyperextension to continental subduction. *Journal of Structural Geology*, *138*, 104122. https://doi.org/10.1016/j.jsg.2020.104122
Platt, J. P. (2007). From orogenic hinterlands to Mediterranean-style back-arc basins: A comparative analysis. *Journal of the Geological Society*, *164*(2), 297–311. https://doi.org/10.1144/0016-76492006-093
Platt, J. P., Anczkiewicz, R., Soto, J.-I., Kelley, S. P., & Thirlwall, M. (2006). Early Miocene continental subduction and rapid exhumation in the western Mediterranean. *Geology*, *34*(11), 981–984. https://doi.org/10.1130/G22801A.1
Platt, J. P., Argles, T. W., Carter, A., Kelley, S. P., Whitehouse, M. J., & Lonergan, L. (2003a). Exhumation of the Ronda peridotite and its crustal envelope: Constraints from thermal modeling of a P-T-time array. *Journal of the Geological Society*, *160*(5), 655–676. https://doi.org/10.1144/0016-764902-108
Platt, J. P., Behr, W. M., Johanesen, K., & Williams, J. R. (2013). The Betic-Rif Arc and its orogenic hinterland: A review. *Annual Review of Earth and Planetary Sciences*, *41*(1), 313–357. https://doi.org/10.1146/annurev-earth-050212-123951
Platt, J. P., Kelley, S. P., Carter, A., Orozco, M. (2005). Timing of tectonic events in the Alpujarride Complex, Betic Cordillera, southern Spain. *Journal of the Geological Society*, *162*(3), 451–462. https://doi.org/10.1144/0016-764903-039
Platt, J. P., Soto, J.-I., Whitehouse, M. J., Hurford, A. J., & Kelley, S. P. (1998). Thermal evolution, rate of exhumation, and tectonic significance of metamorphic rocks from the floor of the Alboran extensional basin, western Mediterranean. *Tectonics*, *17*(5), 671–689. https://doi.org/10.1029/98TC02204
Platt, J. P., & Vissers, R. L. M. (1989). Extensional collapse of thickened continental lithosphere: A working hypothesis for the Alboran Sea and Gibraltar arc. *Geology*, *17*(6), 540–543. https://doi.org/10.1130/0091-7613(1989)017<0540:ECOTCL>2.3.CO;2
Platt, J. P., & Whitehouse, M. J. (1999). Early Miocene high-temperature metamorphism and rapid exhumation in the Betic Cordillera (Spain): Evidence from U-Pb zircon ages. *Earth and Planetary Science Letters*, *171*(4), 591–605. https://doi.org/10.1016/S0012-821X(99)00176-4
Platt, J. P., Whitehouse, M. J., Kelley, S. P., Carter, A., & Hollick, L. (2003b). Simultaneous extensional exhumation across the Alboran Basin: Implications for the causes of late orogenic extension. *Geology*, *31*(3), 251–254. https://doi.org/10.1130/0091-7613(2003)031<0251:SEEATA>2.0.CO;2
Priem, H. N. A., Boelrijk, N. A. I. M., Hebeda, E. H., Oen, I. S., Verdurmen, E. T., & Verschure, R. H. (1979). Isotopic dating of the emplacement of the ultramafic masses in the Serrania de Ronda, southern Spain. *Contributions to Mineralogy and Petrology*, *70*(1), 103–109. https://doi.org/10.1007/BF00371876
Puga, E., Nieto, J. M., de Federico, A. D., Bodinier, J. A., & Morten, L. (1999). Petrology and metamorphic evolution of ultramafic rocks and dolerite dykes of the Betic Ophiolitic Association (Mulhacén Complex, SE Spain): Evidence of eo-Alpine subduction following an ocean-floor metasomatic process. *Lithos*, *49*(1–4), 23–56. https://doi.org/10.1016/S0024-4937(99)00035-3
Rodríguez-Ruiz, M. D., Abad, I., & Bentabol, M. J. (2019). Permo-Triassic clastic rocks from the Ghomaride complex and Federico units (Rif Cordillera, N Morocco): An example of diagenetic-metamorphic transition. *Minerals*, *9*(12), 738. https://doi.org/10.3390/min9120738
Romagny, A., Jolivet, L., Menant, A., Bessière, E., Maillard, A., Canva, A., et al. (2020). Detailed tectonic reconstructions of the Western Mediterranean region for the last 35 Ma, insights on driving mechanisms. *Bulletin de la Societe Geologique de France*, *191*(1), 37. https://doi.org/10.1051/bsgf/2020040
Romagny, A., Münch, P. H., Cornée, J. J., Corsini, M., Azdimousa, A., Melinte-Dobrinescu, M. C., et al. (2014). Late Miocene to present-day exhumation and uplift of the Internal Zone of the Rif chain: Insights from low temperature thermochronometry and basin analysis. *Journal of Geodynamics*, *77*, 39–55. https://doi.org/10.1016/j.jog.2014.01.006

Rosenbaum, G., Lister, G. S., & Duboz, C. (2002). Reconstruction of the tectonic evolution of the western Mediterranean since the Oligocene. *Journal of the Virtual Explorer*, *8*, 107–130. https://doi.org/10.3809/jvirtex.2002.00053

Rossetti, F., Dini, A., Lucci, F., Bouybaouene, M. L., & Faccenna, C. (2013). Early Miocene strike-slip tectonics and granite emplacement in the Alboran Domain (Rif Chain, Morocco): Significance for the geodynamic evolution of Western Mediterranean. *Tectonophysics*, *608*, 774–791. https://doi.org/10.1016/J.TECTO.2013.08.002

Rossetti, F., Faccenna, C., & Crespo-Blanc, A. (2005). Structural and kinematic constraints to the exhumation of the Alpujarride Complex (Central Betic Cordillera, Spain). *Journal of Structural Geology*, *27*(2), 199–216. https://doi.org/10.1016/j.jsg.2004.10.008

Rossetti, F., Faccenna, C., Goffé, B., Monié, P., Argentieri, A., Funiciello, R., & Mattei, M. (2001). Alpine structural and metamorphic signature of the Sila Piccola Massif nappe stack (Calabria, Italy): Insights for the tectonic evolution of the Calabrian Arc. *Tectonics*, *20*(1), 112–133. https://doi.org/10.1029/2000TC900027

Rossetti, F., Goffé, B., Monié, P., Faccenna, C., & Vignaroli, G. (2004). Alpine orogenic P-T-t-deformation history of the Catena Costiera area and surrounding regions (Calabrian Arc, southern Italy): The nappe edifice of north Calabria revised with insights on the Tyrrhenian-Apennine system formation. *Tectonics*, *23*, TC6011. https://doi.org/10.1029/2003TC001560

Rossetti, F., Lucci, F., Theye, T., Bouybaouene, M. L., Gerdes, A., Opitz, J., et al. (2020). Hercynian anatexis in the envelope of the Beni Bousera peridotites (Alboran Domain, Morocco): Implications for the tectono-metamorphic evolution of the deep crustal roots of the Mediterranean region. *Gondwana Research*, *83*, 157–182. https://doi.org/10.1016/j.gr.2020.01.020

Rossetti, F., Theye, T., Lucci, F., Bouybaouene, M. L., Dini, A., Gerdes, A., et al. (2010). Timing and modes of granite magmatism in the core of the Alboran Domain, Rif chain, northern Morocco: Implications for the Alpine evolution of the western Mediterranean. *Tectonics*, *29*, TC2017. https://doi.org/10.1029/2009TC002487

Royden, L. H. (1993). Evolution of retreating subduction boundaries formed during continental collision. *Tectonics*, *12*(3), 629–638. https://doi.org/10.1029/92TC02641

Ruiz Cruz, M. D., & Sanz De Galdeano, C. (2013). Coesite and diamond inclusions, exsolution microstructures and chemical patterns in ultrahigh pressure garnet from Ceuta (Northern Rif, Spain). *Lithos*, *177*, 184–206. https://doi.org/10.1016/j.lithos.2013.06.004

Ruiz Cruz, M. D., & Sanz de Galdeano, C. (2014). Garnet variety and zircon ages in UHP meta-sedimentary rocks from the Jubrique zone (Alpujárride Complex, Betic Cordillera, Spain): Evidence for a pre-Alpine emplacement of the Ronda peridotite. *International Geology Review*, *56*(7), 845–868. https://doi.org/10.1080/00206814.2014.904759

Ruiz Cruz, M. D., Sanz De Galdeano, C., Alvarez-Valero, A., Rodriguez Ruiz, M. D., & Novák, J. (2010). Pumpellyite and coexisting minerals in metapelites and veins from the Federico units in the internal zone of the Rif, Spain. *Canadian Mineralogist*, *48*(1), 183–203. https://doi.org/10.3749/canmin.48.1.183

Sánchez-Navas, A., García-Casco, A., & Martín-Algarra, A. (2014). Pre-Alpine discordant granitic dikes in the metamorphic core of the Betic Cordillera: Tectonic implications. *Terra Nova*, *26*(6), 477–486. https://doi.org/10.1111/ter.12123

Sánchez-Navas, A., García-Casco, A., Mazzoli, S., & Martín-Algarra, A. (2017). Polymetamorphism in the Alpujarride complex, Betic Cordillera, South Spain. *Journal of Geology*, *125*(6), 637–657. https://doi.org/10.1086/693862

Sánchez-Rodríguez, L., & Gebauer, D. (2000). Mesozoic formation of pyroxenites and gabbros in the Ronda area (southern Spain), followed by Early Miocene subduction metamorphism and emplacement into the middle crust: U-Pb sensitive high-resolution ion microprobe dating of zircon. *Tectonophysics*, *316*(1–2), 19–44. https://doi.org/10.1016/S0040-1951(99)00256-5

Schenk, V. (1980). U-Pb and Rb-Sr radiometric dates and their correlation with metamorphic events in the granulite facies basement of the Serre, southern Calabria (Italy). *Contributions to Mineralogy and Petrology*, *73*, 23–38. https://doi.org/10.1007/BF00376258

Serrano, F., Sanz de Galdeano, C., El Kadiri, K., Guerra-Merchán, A., López-Garrido, A. C., Martín-Martín, M., & Hlila, R. (2006). Oligocene-early Miocene transgressive cover of the Betic-Rif Internal Zone. Revision of its geologic significance. *Eclogae Geologicae Helvetiae*, *99*(2), 237–253. https://doi.org/10.1007/s00015-006-1186-9

Simancas, J. F., & Campos, J. (1993). Compresión NNW-SSE tardi a postmetamórfica y extensión subordinada en el Complejo Alpujárride (Dominio de Alborán, Orógeno Bético). *Revista de la Sociedad Geologica de Espana*, *6*(1–2), 23–25.

Sosson, M., Morrillon, A. C., Bourgois, J., Féraud, G., Poupeau, G., & Saint-Marc, P. (1998). Late exhumation stages of the Alpujarride Complex (western Betic Cordilleras, Spain): New thermochronological and structural data on Los Reales and Ojen nappes. *Tectonophysics*, *285*(3–4), 253–273. https://doi.org/10.1016/S0040-1951(97)00274-6

Soto, J.-I., & Platt, J. P. (1999). Petrological and structural evolution of high-grade metamorphic rocks from the floor of the Alboran Sea basin, western Mediterranean. *Journal of Petrology*, *40*(1), 21–60. https://doi.org/10.1093/petrology/40.1.21

Spakman, W., & Wortel, R. (2004). A tomographic view on western Mediterranean geodynamics. In *The TRANSMED atlas. The Mediterranean region from crust to mantle* (pp. 31–52). Berlin Springer. https://doi.org/10.1007/978-3-642-18919-7_2

Stipp, M., Stünitz, H., Heilbronner, R., & Schmid, S. M. (2002). Dynamic recrystallization of quartz: Correlation between natural and experimental conditions. *Geological Society, London, Special Publications*, *200*, 171–190. https://doi.org/10.1144/GSL.SP.2001.200.01.11

Tubía, J. M., Cuevas, J., & Esteban, J. J. (2004). Tectonic evidence in the Ronda peridotites, Spain, for mantle diapirism related to delamination. *Geology*, *32*(11), 941–944. https://doi.org/10.1130/G20869.1

Tubía, J. M., Cuevas, J., & Ibarguchi, J. G. (1997). Sequential development of the metamorphic aureole beneath the Ronda peridotites and its bearing on the tectonic evolution of the Betic Cordillera. *Tectonophysics*, *279*(1–4), 227–252. https://doi.org/10.1016/S0040-1951(97)00124-8

Tubía, J. M., Cuevas, J., Navarro-Vilá, F., Alvarez, F., & Aldaya, F. (1992). Tectonic evolution of the Alpujárride Complex (Betic Cordillera, southern Spain). *Journal of Structural Geology*, *14*(2), 193–203. https://doi.org/10.1016/0191-8141(92)90056-3

Turner, S. P., Platt, J. P., George, R. M. M., Kelley, S. P., Pearson, D. G., & Nowell, G. M. (1999). Magmatism associated with orogenic collapse of the Betic-Alboran Domain, SE Spain. *Journal of Petrology*, *40*(6), 1011–1036. https://doi.org/10.1093/petroj/40.6.1011

van der Pluijm, B. A., Hall, C. M., Vrolijk, P. J., Pevear, D. R., & Covey, M. C. (2001). The dating of shallow faults in the Earth's crust. *Nature*, *412*(6843), 172–175. https://doi.org/10.1038/35084053

van Hinsbergen, D. J., Torsvik, T. H., Schmid, S. M., Maţenco, L. C., Maffione, M., Vissers, R. L., et al. (2020). Orogenic architecture of the Mediterranean region and kinematic reconstruction of its tectonic evolution since the Triassic. *Gondwana Research*, *81*, 79–229. https://doi.org/10.1016/j.gr.2019.07.009

van Hinsbergen, D. J., Vissers, R. L. M., & Spakman, W. (2014). Origin and consequences of western Mediterranean subduction, rollback, and slab segmentation. *Tectonics*, *33*(4), 393–419. https://doi.org/10.1002/2013TC003349

Vergés, J., & Fernàndez, M. (2012). Tethys-Atlantic interaction along the Iberia-Africa plate boundary: The Betic-Rif orogenic system. *Tectonophysics*, *579*, 144–172. https://doi.org/10.1016/j.tecto.2012.08.032

Vermeesch, P. (2018). IsoplotR: A free and open toolbox for geochronology. *Geoscience Frontiers*, *9*(5), 1479–1493. https://doi.org/10.1016/j.gsf.2018.04.001

Vidal, O., & Goffé, B. (1991). Cookeite $LiAl_4(Si_3Al)O_{10}(OH)_8$: Experimental study and thermodynamical analysis of its compatibility relations in the $Li_2O$-$Al_2O_3$-$SiO_2$-$H_2O$ system. *Contributions to Mineralogy and Petrology*, *108*(1–2), 72–81. https://doi.org/10.1093/petrology/egm00210.1007/bf00307327

Vidal, O., Goffé, B., Bousquet, R., & Parra, T. (1999). Calibration and testing of an empirical chloritoid-chlorite Mg-Fe exchange thermometer and thermodynamic data for daphnite. *Journal of Metamorphic Geology*, *17*(1), 25–39. https://doi.org/10.1046/j.1525-1314.1999.00174.x

Vidal, O., Goffé, B., & Theye, T. (1992). Experimental study of the stability of sudoite and magnesiocarpholite and calculation of a new petrogenetic grid for the system FeO-MgO-$Al_2O_3$-$SiO_2$-$H_2O$. *Journal of Metamorphic Geology*, *10*(5), 603–614. https://doi.org/10.1093/petrology/egm002

Vignaroli, G., Minelli, L., Rossetti, F., Balestrieri, M. L., & Faccenna, C. (2012). Miocene thrusting in the eastern Sila Massif: Implication for the evolution of the Calabria-Peloritani orogenic wedge (southern Italy). *Tectonophysics*, *538*, 105–119. https://doi.org/10.1016/j.tecto.2012.03.011

Vignaroli, G., Rossetti, F., Theye, T., & Faccenna, C. (2008). Styles and regimes of orogenic thickening in the Peloritani Mountains (Sicily, Italy): New constraints on the tectono-metamorphic evolution of the Apennine belt. *Geological Magazine*, *145*(4), 552–569. https://doi.org/10.1017/S0016756807004293

Villa, I. M., Bucher, S., Bousquet, R., Kleinhanns, I. C., & Schmid, S. M. (2014). Dating polygenetic metamorphic assemblages along a transect across the Western Alps. *Journal of Petrology*, *55*(4), 803–830. https://doi.org/10.1093/petrology/egu007

Vitale, S., Zaghloul, M. N., El Ouaragli, B., Tramparulo, F. D. A., & Ciarcia, S. (2015). Polyphase deformation of the Dorsale Calcaire Complex and the Maghrebian Flysch Basin Units in the Jebha area (Central Rif, Morocco): New insights into the Miocene tectonic evolution of the Central Rif belt. *Journal of Geodynamics*, *90*, 14–31. https://doi.org/10.1016/j.jog.2015.07.002

Wessel, P., Smith, W. H. F., Scharroo, R., Luis, J., & Wobbe, F. (2013). Generic mapping tools: Improved version released. *Eos, Transactions, American Geophysical Union*, *94*, 409–410. https://doi.org/10.1002/2013eo450001

Whitney, D. L., & Evans, B. W. (2010). Abbreviations for names of rock-forming minerals. *American Mineralogist*, *95*(1), 185–187. https://doi.org/10.2138/am.2010.3371

Wildi, W. (1983). La chaîne tello-rifaine (Algérie, Maroc, Tunisie): Structure, stratigraphie et évolution du Trias au Miocène. *Revue de Geographie Physique et de Geologie Dynamique*, *24*(3), 201–297.

Williams, J. R., & Platt, J. P. (2018). A new structural and kinematic framework for the Alborán Domain (Betic-Rif arc, western Mediterranean orogenic system). *Journal of the Geological Society*, *175*(3), 465–496. https://doi.org/10.1144/jgs2017-086

Zaghloul, M. N. (1994). *Les unités Federico septentrionales (Rif interne, Maroc) inventaire des déformations et contexte géodynamique Thèse, Diplôme Etudes Supérieures*. Université Mohammed V.

Zaghloul, M. N., Critelli, S., Perri, F., Mongelli, G., Perrone, V., Sonnino, M., et al. (2010). Depositional systems, composition and geochemistry of Triassic rifted-continental margin redbeds of the Internal Rif Chain, Morocco. *Sedimentology*, *57*, 312–350. https://doi.org/10.1111/j.1365-3091.2009.01080.x

Zaghloul, M. N., Di Staso, A., El Moutchou, B., Gigliuto, L. G., & Puglisi, D. (2005). Sedimentology, provenance and biostratigraphy of the Upper Oligocene-Lower Miocene terrigenous deposits of the internal "Dorsale Calcaire" (Rif, Morocco): Palaeogeographic and geodynamic implications. *Bollettino della Societa Geologica Italiana*, *124*, 437–454.

Zeck, H. P. (1996). Betic-Rif orogeny: Subduction of Mesozoic Tethys lithosphere under eastward drifting Iberia, slab detachment shortly before 22 Ma, and subsequent uplift and extensional tectonics. *Tectonophysics*, *254*(1–2), 1–16. https://doi.org/10.1016/0040-1951(95)00206-5

Zeck, H. P., Monie, P., Villa, I. M., & Hansen, B. T. (1992). Very high-rates of cooling and uplift in the alpine belt of the Betic Cordilleras, Southern Spain. *Geology*, *20*(11), 1053–1054. https://doi.org/10.1130/0091-7613(1992)020<0079:VHROCA>2.3.CO;2

Zeck, H. P., & Whitehouse, M. J. (2002). Repeated age resetting in zircons from Hercynian-Alpine polymetamorphic schists (Betic-Rif tectonic belt, S. Spain)—A U-Th-Pb ion microprobe study. *Chemical Geology*, *182*, 275–292. https://doi.org/10.1016/S0009-2541(01)00296-0

Zeck, H. P., & Williams, I. S. (2001). Hercynian metamorphism in nappe core complexes of the Alpine Betic-Rif Belt, Western Mediterranean-a SHRIMP Zircon Study. *Journal of Petrology*, *42*(7), 1373–1385. https://doi.org/10.1093/petrology/42.7.1373

## Reference From the Supporting Information

Berger, G. W., & York, D. (1970). Precision of the $^{40}Ar/^{39}Ar$ dating technique. *Earth and Planetary Science Letters*, *9*(1), 39–44. https://doi.org/10.1016/0012-821X(70)90021-X

Brandelik, A. (2009). CALCMIN—An EXCEL™ Visual Basic application for calculating mineral structural formulae from electron microprobe analyses. *Computers & Geosciences*, *35*(7), 1540–1551. https://doi.org/10.1016/j.cageo.2008.09.011

Hall, C. M. (2014). Direct measurement of recoil effects on $^{40}Ar/^{39}Ar$ standards. *Geological Society, London, Special Publications*, *378*(1), 53–62. https://doi.org/10.1144/SP378.7

Lee, J. Y., Marti, K., Severinghaus, J. P., Kawamura, K., Yoo, H. S., Lee, J. B., & Kim, J. S. (2006). A redetermination of the isotopic abundances of atmospheric Ar. *Geochimica et Cosmochimica Acta*, *70*(17), 4507–4512. https://doi.org/10.1016/j.gca.2006.06.1563

Ludwig, K. R. (2003). User's manual for IsoPlot 3.0: A geochronological toolkit for Microsoft Excel, 71.

Phillips, G., Wilson, C. J., Phillips, D., & Szczepanski, S. K. (2007). Thermochronological ($^{40}Ar/^{39}Ar$) evidence of Early Palaeozoic basin inversion within the southern Prince Charles Mountains, East Antarctica: Implications for East Gondwana. *Journal of the Geological Society*, *164*(4), 771–784. https://doi.org/10.1144/0016-76492006-073

Renne, P. R., Balco, G., Ludwig, K. R., Mundil, R., & Min, K. (2011). Response to the comment by WH Schwarz et al. on "Joint determination of $^{40}K$ decay constants and $^{40}Ar^*/^{40}K$ for the Fish Canyon sanidine standard, and improved accuracy for $^{40}Ar/^{39}Ar$ geochronology" by PR Renne et al. (2010). *Geochimica et Cosmochimica Acta*, *75*(17), 5097–5100. https://doi.org/10.1016/j.gca.2011.06.021

Renne, P. R., Swisher, C. C., Deino, A. L., Karner, D. B., Owens, T. L., & DePaolo, D. J. (1998). Intercalibration of standards, absolute ages and uncertainties in $^{40}Ar/^{39}Ar$ dating. *Chemical Geology*, *145*(1–2), 117–152. https://doi.org/10.1016/S0009-2541(97)00159-9